

Nonlinear compressive reduced basis approximation : when Taylor meets Kolmogorov

Joubine Aghili^{1,2}, Hassan Ballout ^{*1}, Yvon Maday³, and Christophe Prud'homme¹

¹IRMA, Université de Strasbourg, CNRS UMR 7501, 7 rue René Descartes, 67084 Strasbourg, France

²INRIA Nancy-Grand Est, MACARON Project, Strasbourg, France

³Sorbonne Université, CNRS, Université Paris Cité, Laboratoire Jacques-Louis Lions (LJLL), F-75005 Paris, France

2026

Abstract

This paper investigates a class of model reduction methods for efficiently approximating the solution of parameter-dependent partial differential equations, where the parameter is a multi-parameter vector $\mu \in \mathbb{R}^p$. In classical settings where the Kolmogorov N -width decays sufficiently fast, it is effective to approximate the solution as a sum of N separable terms, each being the product of a parameter-dependent coefficient and a space- (or space-time-) dependent function. This leads to reduced-order models with N degrees of freedom and computational complexity of order $\mathcal{O}(N^3)$.

However, when the Kolmogorov N -width decays slowly, N must be large to achieve acceptable accuracy, and such cubic complexity becomes prohibitive. The linear complexity measure in terms of Kolmogorov N -width has to be replaced by a more involved width: the Gelfand width for instance with its associated notion of sensing number. Recent nonlinear reduction approaches based on this notion have proposed to decompose the N coordinates into two groups: n free variables and \bar{n} dependent variables, where the latter are expressed as nonlinear functions of the former and $N = n + \bar{n}$. Several works have focused on the case where these \bar{n} functions are homogeneous quadratic forms of the n main variables, with optimization strategies for choosing n given a target accuracy.

The main contribution of this paper is a rigorous analysis of the local sensing number, showing that the optimal choice $n = p$ is appropriate when the parameter variations remain locally concentrated around a reference point. In practical scenarios involving wide parameter ranges, the condition $p \leq n \leq p + k$ (with k small) is valid and more robust from continuity arguments. Additionally, the assumption of a quadratic mapping, also justified in a local sense, becomes insufficient. More expressive nonlinear mappings — including those learned from data using machine learning — become necessary.

This work contributes a theoretical foundation for such nonlinear reduction strategies and highlights the need for further investigations into their reliability, interpretability, and safeguards, particularly in order to apply this type of approach and push back the Kolmogorov Barrier.

Contents

1	Introduction	2
2	Linear approximation and reduced basis construction	5
2.1	Singular Value Decomposition	6
2.2	Greedy Algorithms	8
2.3	GSS: Greedy-Sampled SVD	9

^{*}hassan.ballout@math.unistra.fr, corresponding author

3	Nonlinear approximation	10
3.1	Nonlinear widths	11
3.2	Nonlinear Compressive Reduced Basis Approximation	12
4	Approximation with Taylor polynomial expansions	13
4.1	Notations and Assumptions	13
4.2	Tangent space of the centered manifold	13
4.2.1	Convergence of the first order modes	14
4.2.2	Convergence of the coefficients	15
4.2.3	Local invertibility of the coefficient map	16
4.2.4	Sensing numbers	18
4.3	Second order Taylor expansion of the centered manifold	20
4.3.1	Convergence of the filtered second-order SVD modes	20
4.3.2	Quadratic law for the limit curvature frame coefficients	21
4.3.3	Quadratic law for the <i>filtered</i> curvature coefficients	22
5	Discussion on quadratic approximation	23
5.1	Description of the quadratic approximation	23
5.2	Problem formulation	24
5.3	Need for full quadratic ansatz	24
6	Numerical illustrations	25
6.1	Test case: A multiparameter problem	25
6.2	GSS	26
6.3	Convergence towards the Taylor expansion	27
6.3.1	Differentiation with respect to the parameter	27
6.3.2	Convergence of the SVD modes	28
6.4	Recovering the high RB modes from the low ones	29
6.5	Enhanced approximation with full quadratic ansatz	30
7	Conclusion	31
A	Different notions of principal angles and the connection with Davis–Kahan $\sin \Theta$ Theorem	32
B	SVD modes convergence	34
B.1	Problem statement	34
B.2	Non-uniqueness of SVD modes	34
B.3	Convergence up to orthogonal transformation	35

1 Introduction

Complexity reduction methods for parameterized systems have received increasing attention in recent years, particularly in the context of approximating solutions to parameterized problems modeled by partial differential equations (PDEs) or data assimilation. These methods often rely, directly or indirectly, on the notion of Kolmogorov N -width of some abstract set of solutions, which provides the optimal framework for achieving reduction using linear approximations. Reduced basis methods have sometimes been presented as a way to mitigate, at least for certain classes of problems, Bellman’s “curse of dimensionality.” The underlying argument is that for many parametrized partial differential equations, the set of solutions does not fill the ambient high-dimensional function space, but rather concentrates on an intrinsically low-dimensional manifold [57, 12, 58, 41, 50]. This was demonstrated by Cohen and DeVore [23] by linking the rapid decrease in the Kolmogorov N -width of certain families of solutions to their regularity as a function of the parameters of the problem. Thus, when the N -width decays exponentially fast, reduced basis methods can indeed break the computational burden that would otherwise be associated with Bellman’s curse.

As a result, in many cases, particularly for elliptic or parabolic problems, the associated Kolmogorov N -width decays rapidly with N , the dimension of the linear space, allowing effective reduction methods to be employed. However, another concept of “curse” has quickly emerged, not related to the combinatorial explosion with dimension, but the insufficient linear expressiveness in the face of a manifold of inherently nonlinear solutions. This is the case, e.g. when problems exhibit convection phenomena or the parameter space becomes large, the decay of the Kolmogorov N -width is significantly slowed down, which impedes vanilla linear subspace approximations. Consequently, for a desired precision, traditional reduction methods may lose competitiveness compared to classical approximation techniques (such as continuous or discontinuous finite elements, finite volume methods, or spectral methods). This issue is known as the *Kolmogorov barrier* (see, e.g. [2, 55, 10]).

The underlying idea behind reduction methods is to observe that classical approximation methods are versatile in the sense that the same method is capable of approximating PDE solutions in a wide range of applications, including fluid dynamics, structural mechanics, and wave propagation. On the contrary, if we focus on a specific class of problems characterized by a partial differential equation (PDE) parameterized, expressed in residual form as find $u(\boldsymbol{\mu}) \in X$ s.t.

$$\mathfrak{R}(u(\boldsymbol{\mu}); \boldsymbol{\mu}) = 0, \quad (1)$$

where X is a given Hilbert space, this versatility may hinder the efficiency of the method. The solution manifold is then $\mathcal{S} := \{u(\boldsymbol{\mu}) \in X \mid \boldsymbol{\mu} \in \mathcal{P}\} \subset X$, which is the set of all solutions $u(\boldsymbol{\mu})$ as the parameter $\boldsymbol{\mu} = (\mu_1, \mu_2, \dots, \mu_p)$ varies over the admissible parameter set $\mathcal{P} \subset \mathbb{R}^p$, one can look for a tailored sequence of discrete spaces that aligns with this objective. Such a method will not perform well for other types of problems, but is optimized for the given parameterized system (1). To achieve this, when the (linear) Kolmogorov N -width is not small, one may adopt a more sophisticated framework for complexity reduction, transitioning from linear to nonlinear approaches.

Before presenting the Nonlinear Compressive Reduced Basis Approximation (NCRBA) method, we will first briefly review the main strategies for overcoming the Kolmogorov barrier in transport problems. We will not dwell too much on local strategies based on piecewise linear approximations of the solution manifold by introducing adaptability, where we refer e.g. to [4, 30, 51, 61, 20, 17, 47, 5, 54, 36], but will focus on global approaches where appropriate intrinsic nonlinear transformations can be used to rectify the manifold of solutions. In the context of transport-dominated problems, where the Kolmogorov N -width of the solution manifold decays only as $\mathcal{O}(1/\sqrt{N})$, linear model reduction techniques often fail to provide efficient approximations. One of the earliest attempts to overcome this limitation via transformations of the physical domain can be traced back to Ohlberger and Rave’s pioneering work on nonlinear approximation spaces [53]. Since then, several transformation-based strategies have been proposed to improve the approximability of the solution manifold. Notably, several methods exploit information on characteristic lines to define nonlinear Lagrangian mappings [52, 59, 49]. An alternative approach, grounded in the theory of integrable systems, involves constructing a time-dependent test basis via Schrödinger operator Lax pairs [38].

A broader and increasingly influential class of techniques is based on optimal transport theory to align solution snapshots and reduce variability across the parameter space [43, 14, 31, 60, 44]. Closely related are registration-based methods, which reinterpret the transport problem as a geometric alignment task and apply variational approaches to learn optimal deformation maps [64, 32].

In the field of nonlinear structural dynamics, an innovative reduction strategy was introduced in [45]. It relies on representing the solution as the sum of two contributions: a first component lying in the tangent subspace spanned by the vibration modes, and a second contribution expressed as a homogeneous quadratic correction involving modal derivatives. This leads to the following parameterization:

$$\tilde{\mathbf{u}}(\boldsymbol{\mu}) = \mathbf{u}_{\text{ref}} + \mathbf{V}\mathbf{q}(\boldsymbol{\mu}) + \mathbf{W}\mathbf{q}(\boldsymbol{\mu})\mathbf{q}(\boldsymbol{\mu})^\top, \quad (2)$$

where \mathbf{V} collects the dominant modes, and the symmetric matrix \mathbf{W} encodes the curvature of the manifold through modal derivative information.

More recently, inspired by both a priori knowledge-based constructions and a posteriori data-driven recognition strategies, several works—starting with the pioneering contribution of Lee and Carlberg [48]—have explored machine-learning-based nonlinear model reduction. These approaches exploit deep architectures such as convolutional autoencoders to learn encoders, decoders, or both, in order to parameterize low-dimensional manifolds. Several alternative methodologies have emerged to address this nonlinear complexity

in reduced basis methods based on different aspects of advanced machine learning techniques. For instance, Franco et al. [33] and Vitullo et al. [66] explored neural network-based strategies for problems with microstructural complexity, demonstrating their potential for accurate and efficient model reduction. Other notable contributions include the operator inference framework by Kramer et al. [46], which directly learns nonlinear reduced models from data. Despite these advancements, existing methods often require a large amount of data to effectively train the neural network and provide a reliable and robust approximation of the solution. Furthermore, current approaches frequently require learning all the modes, which increases computational demands, expands training set sizes, and may introduce potential instability.

Remarkably, as highlighted in [34], some of these methods do not even require solving the underlying parametric equation in the online stage. In parallel, manifold-based approaches similar in spirit to (2) have emerged, but with \mathbf{V} and \mathbf{W} now obtained through learning instead of analytical derivation [10, 37]. Further refinements and performance enhancements have been proposed, for instance in [62]. It is important to note at this stage that these methods are not associated with a posteriori error estimates, which would allow the approximation to be certified or even the error to be quantified.

In this context, the Nonlinear Compressive Reduced Basis Approximation (NCRBA) method, inspired by the notions of *Gelfand width* (with its associated notion of sensing number) and *nonlinear Kolmogorov N -width*, see [28], has been introduced in Barnett et al. [11], Cohen et al. [24]. This approach builds on the observation that, when a solution is expressed in a linear reduced basis (such as one arising from a Kolmogorov-type approach, as previously described, but leading to an approximation of size N , which may be too large to be practical), actually only the first few n coefficients in this basis represent genuine degrees of freedom. The remaining $N - n$ coefficients, though necessary for the desired approximation accuracy, are not independent variables but can be deduced from the first n coefficients via a functional relationship. The primary challenge thus lies in establishing a methodology that enables the reconstruction of the $N - n$ higher-order coefficients from the n fundamental coefficients.

Note that, as a general rule, the effectiveness of nonlinear approximation methods relies on the accurate estimation of tangent spaces to the underlying solution manifold \mathcal{S} . This geometric perspective has deep roots in manifold learning theory, where tangent space estimation has been extensively studied. The work of Tyagi et al. [65] established theoretical foundations for tangent space estimation on smooth Riemannian manifolds using local principal component analysis (PCA), providing convergence guarantees under specific sampling conditions. These results were subsequently strengthened by Aamari and Levraud [1], who derived optimal non-asymptotic convergence for \mathcal{C}^k manifolds. Recent advances have incorporated curvature-aware methods, such as the CA-PCA approach proposed by Gilbert and O'Neill [39], which adapt to local manifold geometry for improved estimation accuracy. These geometric insights directly inform the selection and construction of reduced basis components in our approach, where the coefficients associated with the first n modes correspond to coordinates in the estimated tangent space of the solution manifold.

This paper presents several key contributions that advance both the theoretical understanding and practical implementation of the NCRBA method, which continues the study of the method and extends the understanding of its theoretical formalism of Ballout et al. [9]. In particular, we answer the question of choosing the number n of reduced basis modes based on the number of parameters p on which the problem depends.

Specifically:

- a. We establish a theoretical link between the NCRBA method and the classical Taylor series expansion to rigorously justify the selection of the first reduced basis components as genuine degrees of freedom. While existing work, such as that by Lee and Carlberg [48], effectively applies neural networks for nonlinear approximation, our method improves robustness by anchoring the choice of reduced basis components in the well-established Taylor series theory. This connection ensures that our approach achieves a stable and efficient representation across a wide range of parameter variations.
- b. Our analysis reveals that, at least locally, the number of effective modes (expressed in terms of sensing number) — or degrees of freedom — coincides with the dimension of the parameter space. This provides a stronger theoretical foundation than previously employed heuristic methods. In our context, our results on the sensing number complement those established by Franco et al. [33] related to the nonlinear Kolmogorov width.

- c. We demonstrate that polynomial approximations, although effective locally, have limited validity in broader parameter spaces. This observation highlights a key limitation of polynomial-based reduction approaches and underscores the need for adaptable, localized methods, such as the NCRBA.
- d. By establishing a parallel between the NCRBA method and the concept of sensing number in nonlinear Kolmogorov theory, we strengthen the theoretical foundation of our approach and enhance its predictive capability in scenarios where traditional Kolmogorov methods are limited.
- e. We argue that our targeted learning approach, which focuses on high-energy modes rather than attempting to learn all possible modes, significantly improves efficiency. Since these dominant modes decay in absolute value, our method requires a smaller training dataset compared to techniques that indiscriminately attempt to learn all modes or even the solution itself expressed in classical approximation basis sets. This improvement addresses major challenges faced by earlier neural network-based strategies, which can suffer from data inefficiency and instability when approximating low-energy modes. Note the extension to the NCRBA method we have proposed following this argument in [8].

Recall that we are considering the case where the Kolmogorov N -width decays slowly, implying that the optimal linear subspace minimizing the worst-case projection error is of large dimension, and, in practice, generally not accessible. The goal of the preliminary stage of any reduced basis technology is thus to construct a surrogate reduced space that approximates this optimal subspace as closely as possible, while carefully avoiding unnecessary increases in dimension beyond what is required to meet the target accuracy.

Several strategies have been proposed for this purpose, often as a decisive offline step that governs the efficiency of subsequent reduced-order modeling. For a fixed reduced dimension, the resulting model accuracy can differ by orders of magnitude depending on the method used to build the reduced basis. The literature typically distinguishes two broad methodological families: one, inspired by statistical and machine learning approaches, constructs the reduced space from snapshots shifted by a reference solution (centered manifolds); the other directly addresses the uncentered solution manifold, treating the full set of states as a geometric object to be compressed. This is the reason why, in Section 2, we briefly recall two main classes of methods to construct the reduced basis: the SVD or POD approach and the greedy algorithm. We propose a combined method that we call the Greedy-Sampled SVD method, which appears to be simple to implement and improves both approaches.

The subsequent sections of this paper are organized as follows. In Section 2, we succinctly revisit two primary classes of methods for constructing a reduced basis: the Singular Value Decomposition (SVD) approach, often referred to as the Proper Orthogonal Decomposition (POD), and the greedy algorithm. We also propose the *Greedy-Sampled SVD* method, which appears to be simple to implement and takes advantage of the two approaches and improves both. In Section 3, we introduce notions of *nonlinear widths* by means of encoder and decoders, which are essential for defining the NCRBA method. The principal contribution of the paper is developed in Section 4, where we treat the connection between the space spanned by the SVD modes of the solution manifold \mathcal{S} with the first monomials of the Taylor expansion around a given element. The significance of the quadratic terms is underscored in Section 5, where we also present comparative analysis with alternative quadratic methods. Useful results needed in the previous sections are recalled in Section A and Section B. Finally, numerical validations are given within section 6, more precisely: (i) comparison between the Greedy-Sampled SVD and other basis construction methods, (ii) illustrations of the proximity of the space spanned by SVD modes to those spanned by Taylor modes, (iii) an application of the NCLRB method to a 2D parametrized thermal problem, (iv) comparison between multiple quadratic approximations.

2 Linear approximation and reduced basis construction

In this section, we briefly recall the classical framework of linear approximation, together with the notion of the Kolmogorov N -width and the associated optimal reduced spaces for the solution manifold $\mathcal{S} \subset X$ of (1). Note that X is then the “natural” Hilbert space associated with the underlying PDE.

Linear approximation methods aim at approximating the solution manifold \mathcal{S} by an appropriate N -dimensional linear subspace $\mathcal{V}_N \subset X$, commonly referred to as the reduced space. The performance of such

an approximation is quantified by the Kolmogorov N -width, defined by

$$d_N(\mathcal{S}) := \inf_{\substack{\mathcal{V} \subset X \\ \dim(\mathcal{V}) \leq N}} \sup_{u \in \mathcal{S}} \inf_{v \in \mathcal{V}} \|u - v\|_X. \quad (3)$$

Note that, in the Hilbertian setting considered here, the best approximation of any $u \in \mathcal{S}$ in a given subspace \mathcal{V}_N is achieved by its orthogonal projection $P_{\mathcal{V}_N}(u)$.

The quantity $d_N(\mathcal{S})$ characterizes both the optimal approximation error attainable by any linear reduced space of dimension N and the corresponding (generally non-unique) optimal subspaces. In practice, however, determining an optimal subspace \mathcal{V}_N achieving the infimum in (3) is in general an open and computationally intractable problem, even in a Hilbert space framework such as the one considered here.

We therefore focus on two well-established approaches for constructing effective approximations of such optimal reduced spaces, namely the singular value decomposition (SVD) and greedy algorithms, while noting that several other strategies have been proposed in the literature. Finally, we propose an enhanced strategy, the *Greedy-Sampled SVD* (GSS), which combines the advantages of both approaches and aims to provide reduced spaces that are closer to the optimal ones.

In all that follows, we shall assume that we have discretized the problem by a high-fidelity method, with high accuracy, so that we shall identify the exact solution $u(\boldsymbol{\mu})$ of equation (1) with its high-fidelity approximation $u_N(\boldsymbol{\mu})$. In addition $u_N(\boldsymbol{\mu})$ will be represented by a column vector $\mathbf{u}_N(\boldsymbol{\mu}) \in X \cong \mathbb{R}^N$.

2.1 Singular Value Decomposition

While the SVD is a general concept applicable to any matrix \mathbf{S} , in our context, it is applied to a *snapshot matrix* of the form,

$$\mathbf{S} = [\mathbf{s}_1, \dots, \mathbf{s}_M] \in \mathbb{R}^{N \times M},$$

where each column $\mathbf{s}_i = \mathbf{u}_N(\boldsymbol{\mu}^i) \in \mathbb{R}^N$ represents the vector of degrees of freedom associated with the high-fidelity solution of equation (1) for a given parameter $\boldsymbol{\mu}^i \in \mathcal{P}_M$. Here, $\mathcal{P}_M \subset \mathcal{P}$ denotes a finite *training set* of cardinality M , *sufficiently large and suitably chosen* to adequately represent the parameter domain \mathcal{P} . Note that, in general, $N \geq M$, although this is not a mandatory requirement.

The singular value decomposition of \mathbf{S} reads:

$$\mathbf{S} = \mathbf{U} \boldsymbol{\Sigma} \mathbf{Z}^\top, \quad (4)$$

where:

- $\mathbf{U} = [\boldsymbol{\varphi}_1, \dots, \boldsymbol{\varphi}_N] \in \mathbb{R}^{N \times N}$ is an orthogonal matrix whose columns are the so-called left singular vectors of \mathbf{S} .
- $\boldsymbol{\Sigma} \in \mathbb{R}^{N \times M}$ is a “diagonal” matrix containing the singular values $(\sigma_1, \sigma_2, \dots)$, classically ranked in decreasing order, $\sigma_k \geq \sigma_{k+1}$ for all $k = 1, \dots, M-1$.
- $\mathbf{Z} \in \mathbb{R}^{M \times M}$ is an orthogonal matrix whose columns are the so-called right singular vectors of \mathbf{S} .

The “discrete” space X is typically equipped with an inner product of the form

$$(\mathbf{v}, \mathbf{w})_X = \mathbf{v}^\top \mathbf{M} \mathbf{w}, \quad \mathbf{M} \in \mathbb{R}^{N \times N} \text{ being a symmetric positive definite matrix,}$$

it is important to incorporate the *mass matrix* \mathbf{M} in the reduction procedure. We then introduce the *weighted SVD* of the snapshot matrix by considering the factorization

$$\mathbf{M} = \mathbf{L}^\top \mathbf{L},$$

for instance, via a Cholesky decomposition, and computing the standard SVD of the transformed matrix

$$\tilde{\mathbf{S}} = \mathbf{L} \mathbf{S} = \tilde{\mathbf{U}} \tilde{\boldsymbol{\Sigma}} \tilde{\mathbf{Z}}^\top.$$

This yields the matrix $\Phi = \mathbf{L}^{-1}\tilde{\mathbf{U}}$, the columns of which are modes that are orthonormal in the metric induced by \mathbf{M} .

Alternatively, one can also consider the correlation matrix

$$\mathbf{C} = \mathbf{S}^\top \mathbf{M} \mathbf{S} \in \mathbb{R}^{M \times M}.$$

The associated eigenvalue problem

$$\mathbf{C}\mathbf{v}_k = \lambda_k \mathbf{v}_k, \quad k = 1, \dots, M,$$

yields eigenvalues $\lambda_1 \geq \lambda_2 \geq \dots \geq 0$ and eigenvectors $\mathbf{v}_k \in \mathbb{R}^M$. The associated modes in the high-fidelity space are then given by

$$\varphi_k = \frac{1}{\sqrt{\lambda_k}} \mathbf{S} \mathbf{v}_k, \quad (\varphi_k, \varphi_\ell)_X = \delta_{k\ell}.$$

These vectors $\{\varphi_k\}$ are the *Proper Orthogonal Decomposition* (POD) modes and form an orthonormal system with respect to the X -inner product.

These two approaches (eigenvalue problem on \mathbf{C} , or weighted SVD on $\tilde{\mathbf{S}}$) are fully equivalent with $\sigma_k = \sqrt{\lambda_k}$. The former is often preferred in practice because solving the $M \times M$ eigenvalue problem for \mathbf{C} is computationally cheaper than performing an SVD on the full snapshot matrix.

Optimality property. For $N \leq M$, let $\mathcal{V}_N = \text{span}\{\varphi_1, \dots, \varphi_N\}$. This subspace satisfies

$$\sum_{i=1}^M \|\mathbf{s}_i - P_{\mathcal{V}_N}(\mathbf{s}_i)\|_X^2 = \inf_{\substack{\mathcal{W} \subset X \\ \dim(\mathcal{W}) \leq N}} \sum_{i=1}^M \|\mathbf{s}_i - P_{\mathcal{W}}(\mathbf{s}_i)\|_X^2 = \sum_{k=N+1}^M \lambda_k, \quad (5)$$

where $\|\mathbf{v}\|_X^2 = (\mathbf{v}, \mathbf{v})_X$. Thus, \mathcal{V}_N is the best N -dimensional approximation space for the snapshots in the X -norm, which is an optimality property in average (over the set of parameters), *i.e.* $\ell^2(\mathcal{P}_M)$ rather than $\ell^\infty(\mathcal{P}_M)$ involved in the definition in equation (3)

Centered vs. non-centered snapshots. An additional modeling choice concerns whether the snapshots should be *centered* before performing the decomposition. Defining the empirical mean

$$\bar{\mathbf{s}} = \frac{1}{M} \sum_{i=1}^M \mathbf{s}_i,$$

one can either (i) perform the decomposition on the fluctuations $\mathbf{s}_i - \bar{\mathbf{s}}$, or (ii) directly use the raw snapshots \mathbf{s}_i . In applications such as turbulence modeling, fluid dynamics, or signal processing, it is customary to adopt the centered version, so that the modes represent only the fluctuations around the mean field. In contrast, in the context of Reduced Basis Methods (RBM) for parametric PDEs, it is often preferable *not* to center: the reduced space is then built to approximate the entire solution manifold, not just deviations from the mean.

Remark 1. It is worth emphasizing that the general given modal expansion $\mathbf{u}(\boldsymbol{\mu}) = \sum_k \alpha_k(\boldsymbol{\mu}) \varphi_k$ in \mathbb{R}^N for $\boldsymbol{\mu} \in \mathcal{P}$, admits a direct identification with the SVD if *e.g.* the family $\{\varphi_k\}$ is orthonormal in \mathbb{R}^N and the coefficient vectors $\{\alpha_k(\boldsymbol{\mu})\}$ are orthogonal in $L^2(\mathcal{P})$ with specific decay of the norms that provide the unique optimal orthogonal decomposition in the sense of equation (5).

We end this subsection by noting that there is a large literature on various ways of performing that sampling and the calculation of the SVD modes, including the method of snapshots, greedy and adaptive sampling strategies, and more recently the smart use of randomized and probabilistic approaches for large-scale reduced-order modeling, see, *e.g.* [63, 18, 3, 40, 16, 42, 58, 41, 7, 22, 21, 19, 6, 15].

2.2 Greedy Algorithms

Several other widely adopted approaches to construct a reduced space fall within the family of *greedy algorithm*. Unlike the SVD method, these algorithms build the reduced basis iteratively. At each iteration n , a new basis vector is added by selecting the parameter value that maximizes a suitable representation of the X -projection error. This strategy ensures that the reduced space is enriched in the directions where the current reduced model performs worst. Concretely, the greedy procedure requires computing one high-fidelity solution per iteration. Thus, to build a reduced basis of dimension N , only N high-fidelity solves are needed. This represents a significant computational advantage compared to the SVD/POD approach, which typically requires computing $M \gg N$ snapshot solutions in advance.

The various greedy approaches differ in the way this representation of the projection error is performed. Typically, it is based on an *a posteriori error estimator* that provides a surrogate to a projection error on the current reduced space. This evaluation through such a posteriori error estimator leads to the notion of *weak greedy algorithm*. An essential ingredient of the weak greedy algorithm is thus the availability of an error estimator $\Delta_n(\boldsymbol{\mu})$, which evaluates the projection error on the current n -dimensional reduced space \mathcal{V}_n (built in previous iterations), with a cost that is a function of n (say $\mathcal{O}(n^3)$ for instance). Optimally, it should provide a bound for the error induced by projecting the high-fidelity solution $\mathbf{u}_{\mathcal{N}}(\boldsymbol{\mu})$ onto the current reduced space \mathcal{V}_n , *i.e.*, there exists $\gamma \in \mathbb{R}^{+*}$

$$0 < \gamma \leq \frac{\|\mathbf{u}_{\mathcal{N}}(\boldsymbol{\mu}) - P_{\mathcal{V}_n}(\mathbf{u}_{\mathcal{N}}(\boldsymbol{\mu}))\|_X}{\Delta_n(\boldsymbol{\mu})} \leq 1, \quad \forall \boldsymbol{\mu} \in \mathcal{P}. \quad (6)$$

Another essential ingredient to ensure the computational efficiency of the greedy algorithm is, as in Section 2.1, to replace the continuous parameter domain \mathcal{P} by a finite *training set* $\mathcal{P}_M \subset \mathcal{P}$ which can be chosen very large thanks to the marginal cost of the prediction and error estimator. This avoids solving a global optimization problem over \mathcal{P} at each iteration and instead reduces the selection of the next parameter to a discrete search over \mathcal{P}_M , leading to the following enumeration problem:

$$\boldsymbol{\mu}^{(n+1)} = \arg \max_{\boldsymbol{\mu} \in \mathcal{P}_M} \Delta_n(\boldsymbol{\mu}). \quad (7)$$

Then, a high-fidelity solution $\mathbf{u}_{\mathcal{N}}(\boldsymbol{\mu}^{(n+1)})$ is computed and added to the current \mathcal{V}_n .

We present in Algorithm 1, the *weak greedy algorithm* that contains some orthogonalization procedure based on the mass matrix \mathbf{M} (see Algorithm 2). For the efficient construction of the error estimator $\Delta_n(\boldsymbol{\mu})$, we refer the reader to [57].

Algorithm 1 Weak Greedy Algorithm

```

1: Input: Training set  $\mathcal{P}_M \subset \mathcal{P}$ , tolerance  $\varepsilon > 0$ , maximum dimension  $N_{\max}$ , initial parameter  $\boldsymbol{\mu}^{(1)}$ 
2: Output: Basis  $\mathbf{V} \in \mathbb{R}^{\mathcal{N} \times N}$ 
3:  $\mathbf{V} = \emptyset$ ,  $n = 0$ ,  $\Delta = \varepsilon + 1$ 
4: while  $n < N_{\max}$  and  $\Delta > \varepsilon$  do
5:    $n \leftarrow n + 1$ 
6:   Compute  $\mathbf{u}_{\mathcal{N}}(\boldsymbol{\mu}^{(n)})$ 
7:    $\boldsymbol{\varphi}_n = \text{GramSchmidt}(\mathbf{V}, \mathbf{u}_{\mathcal{N}}(\boldsymbol{\mu}^{(n)}), \mathbf{M})$ 
8:    $\mathbf{V} \leftarrow [\mathbf{V}, \boldsymbol{\varphi}_n]$ 
9:   Select  $\boldsymbol{\mu}^{(n+1)} \in \mathcal{P}_M$  such that:

$$\boldsymbol{\mu}^{(n+1)} = \arg \max_{\boldsymbol{\mu} \in \mathcal{P}_M} \Delta_n(\boldsymbol{\mu})$$

10:  Set  $\Delta \leftarrow \Delta_n(\boldsymbol{\mu}^{(n+1)})$ 
11: end while
12:  $N \leftarrow n$ 

```

Algorithm 2 Gram-Schmidt orthonormalization

```

1: function GRAMSCHMIDT( $\mathbf{V}$ ,  $\mathbf{u}$ ,  $\mathbf{M}$ )
2:   if  $\mathbf{V} = []$  then
3:      $\mathbf{z} = \mathbf{u}$ 
4:   else
5:      $\mathbf{z} = \mathbf{u} - \mathbf{V}\mathbf{V}^\top \mathbf{M}\mathbf{u}$ 
6:   end if
7:    $\mathbf{z} \leftarrow \mathbf{z} / \|\mathbf{z}\|_M$ 
8:   return  $\mathbf{z}$ 
9: end function

```

From equation (7), one can clearly observe that the greedy method operates in a *worst-case* sense—namely in the $\ell^\infty(\mathcal{P}_M)$ norm—similar to the Kolmogorov N -width (in $L^\infty(\mathcal{P})$). This contrasts with the SVD-based approach (see section 2.1), which provides an *optimal basis in the mean-square* (*i.e.*, $\ell^2(\mathcal{P}_M)$) sense.

In this direction, the numerical analysis of these algorithms (see [16, 27]) proves that, algebraic (resp. exponential) decay to zero of the Kolmogorov N -width is asymptotically satisfied by the sequence of spaces $\{\mathcal{V}_n\}_n$ obtained by the weak-greedy algorithm, provided that the training sets \mathcal{P}_M are suitably chosen. More precisely, let us introduce a comparable quantity as $d_n(\mathcal{S})$ associated to the series of spaces $\{\mathcal{V}_n\}_n$ defined in the greedy algorithm:

$$\Gamma_n(\mathcal{S}) = \sup_{\boldsymbol{\mu} \in \mathcal{P}_M} \inf_{v_N \in \mathcal{V}_N} \|\mathbf{u}_N(\boldsymbol{\mu}) - v_N\|_X. \quad (8)$$

In particular, it holds that, there exists $\alpha > 0$ such that for any $n \geq 1$, (at least in the limit $M \rightarrow \infty$)

- If $d_n(\mathcal{S}) \leq C_0 n^{-\alpha}$, then $\Gamma_n(\mathcal{S}) \leq C_1 n^{-\alpha}$ with $C_1 = 2^{5\alpha+1} \gamma^{-2} C_0$,
- if $d_n(\mathcal{S}) \leq C_0 e^{-c_0 n^\alpha}$, then $\Gamma_n(\mathcal{S}) \leq \sqrt{2C_0} \gamma^{-1} e^{-c_1 n^\alpha}$ where $c_1 = 2^{-1-2\alpha} c_0$

which is a very powerful result, at least whenever the decay of the Kolmogorov N -width is fast enough.

In this paper, we are rather interested in cases where the Kolmogorov barrier is present and thus we do not have this exponential or geometric rate for $d_n(\mathcal{S})$, we have to be more precise in this comparison, and use the sharper statement also present in the above references (see also [50]): for any $n \geq 1$, we have

$$\Gamma_n(\mathcal{S}) \leq c \gamma^{-1} \min_{1 \leq m \leq n} d_m^{\frac{n-m}{n}}(\mathcal{S}).$$

In particular $\Gamma_{2n}(\mathcal{S}) \leq \sqrt{2} \gamma^{-1} \sqrt{d_n(\mathcal{S})}$, for any $n \geq 1$. This latter bound greatly relativizes the optimality of the greedy method. In fact, it quickly becomes apparent (see *e.g.* the Figure 3 below) that the SVD method provides better approximation results than the greedy methods, at least for small values of n . Indeed, the optimal approaches of Kolmogorov and SVD use first basis functions that mix the (*i.e.*, are linear combinations of many) pure states given by the solutions $\mathbf{u}_N(\boldsymbol{\mu})$ while the greedy methods are based on spaces spanned by pure states.

However, the optimal subspace achieving the Kolmogorov width remains unreachable in practice. Indeed, the greedy algorithm selects one function per iteration, which only yields a *step by step* update to the reduced space rather than performing a global optimization over all N -dimensional subspaces. The next section presents a way to get the best of the greedy and SVD approaches.

2.3 GSS: Greedy-Sampled SVD

In this hybrid approach, we aim to leverage the strengths of both the Greedy algorithm and the SVD. The key idea is to use the Greedy algorithm to select a representative set of parameter-dependent high-fidelity solutions and then apply an SVD to these snapshots in order to extract an optimally compressed basis that mixes the pure states. This two-step strategy allows us to combine: (i) the explorative sampling power of Greedy, (ii) the optimal compression property of SVD.

Let M_1 denote the cardinality of a fine training set $\mathcal{P}_{\text{train}}$, and M_2 the number of Greedy iterations used to select the snapshots. From these M_2 snapshots, we apply SVD and retain the first N left singular vectors

as the reduced basis. Typically, we have $M_1 \gg M_2 > N$. The full procedure is detailed in Algorithm 3. It is important to note that when $M_2 = N$, applying SVD to the Greedy-selected snapshots does not change the reduced space. In this case, both the classical Greedy method and the GSS yield the same N -dimensional subspace, even though the two methods produce *different bases* for that space. We recommend $M_2 = 2N$ as a rule of thumb.

Algorithm 3 GSS

- 1: **Input:** Training set $\mathcal{P}_{\text{train}}$ of size M_1 , number of Greedy iterations M_2 , reduced basis dimension $N < M_2$, initial parameter $\boldsymbol{\mu}^{(1)}$
- 2: **Output:** Basis $\mathbf{V} \in \mathbb{R}^{N \times N}$
- 3: $\mathbf{W} = [\mathbf{u}_{\mathcal{N}}(\boldsymbol{\mu}^{(1)}) / \|\mathbf{u}_{\mathcal{N}}(\boldsymbol{\mu}^{(1)})\|_M, \mathbf{S} = [\mathbf{u}_{\mathcal{N}}(\boldsymbol{\mu}^{(1)})]$
- 4: **for** $n = 2$ to M_2 **do**
- 5: Select $\boldsymbol{\mu}^{(n)} \in \mathcal{P}_{\text{train}}$ such that:
$$\boldsymbol{\mu}^{(n)} = \arg \max_{\boldsymbol{\mu} \in \mathcal{P}_{\text{train}}} \Delta_{n-1}(\boldsymbol{\mu})$$
- 6: Compute $\mathbf{s}_n = \mathbf{u}_{\mathcal{N}}(\boldsymbol{\mu}^{(n)})$
- 7: $\boldsymbol{\xi}_n = \text{GramSchmidt}(\mathbf{W}, \mathbf{s}_n, \mathbf{M})$
- 8: $\mathbf{S} \leftarrow [\mathbf{S}, \mathbf{s}_n]$
- 9: $\mathbf{W} \leftarrow [\mathbf{W}, \boldsymbol{\xi}_n]$, used for computing $\Delta_n(\boldsymbol{\mu})$
- 10: **end for**
- 11: Apply SVD/POD on $\mathbf{S} \in \mathbb{R}^{N \times M_2}$ and extract the first N modes as the basis \mathbf{V} .

Advantages over SVD/POD As discussed in Sections 2.1 and 2.2, a limitation of standard SVD is the need to solve the high-fidelity model over a dense sampling of the parameter space, typically chosen a priori using heuristics (*e.g.*, uniform grid or random sampling). This can lead to inefficient coverage of the parameter domain, especially when the manifold exhibits anisotropic behavior.

In contrast, the GSS approach uses the error estimator to guide the sampling towards the most “informative” parameters, reducing the number of high-fidelity solves $M_2 \ll M_1$ and increasing the relevance of the snapshots. By performing an SVD over these smartly chosen snapshots, the method benefits from both parameter adaptivity and optimal mode compression.

Advantages over Greedy The GSS approach enriches the classical Greedy algorithm by introducing a post-processing compression step based on SVD, which provides an *optimal low-rank approximation* of the selected snapshots, in the sense of equation (5) for $M = M_2$.

As explained above, SVD modes are not just selected pure solutions but *linear combinations of multiple solutions*, enabling the construction of “richer” basis functions. This distinction is particularly beneficial when every snapshot exhibits *localized features*, as is often the case in transport-dominated problems. By combining several locally supported solutions, SVD tends to produce modes that better capture the global behavior of the system.

The GSS approach, therefore, enhances the classical Greedy method by introducing this additional compression and optimality step, without losing the parameter-adaptive strength of the greedy selection strategy. We refer to subsection 6.2 for the illustration of these improvements.

3 Nonlinear approximation

Even if care is taken to select the best possible reduced basis, the span of which is as close as possible to the optimal spaces used in the definition of Kolmogorov N -width, linear approximation techniques may suffer from the *Kolmogorov barrier*, as discussed in Section 2. This is why we turn to *nonlinear approximation* methods, which aim to mitigate this barrier and reduce the associated approximation complexity.

In this section, we first recall some nonlinear notions of width that generalize the classical Kolmogorov N -width to nonlinear settings. We then present a specific approximation technique, namely the *Nonlinear Compressive Reduced Basis Approximation* (NCRBA) method [11, 24, 9], which is the main nonlinear method of interest in this work.

3.1 Nonlinear widths

Model order reduction techniques can be analyzed using the general paradigm of *encoder–decoder* pairs. The goal is to approximate each $u \in \mathcal{S} \subset X$ by a low-dimensional representation using:

- an *encoder* $E : X \rightarrow \mathbb{R}^n$ mapping to a latent space,
- a *decoder* $D : \mathbb{R}^n \rightarrow X$ reconstructing an approximation,

such that $u \approx D(E(u))$. The approximation quality is measured by the worst-case distortion:

$$\mathcal{E}_n(\mathcal{S}; E, D) := \sup_{u \in \mathcal{S}} \|u - D(E(u))\|_X. \quad (9)$$

By minimizing this quantity over admissible encoder–decoder pairs, one obtains different notions of approximation widths.

If no restriction is imposed on E and D beyond continuity (or potentially Lipschitz continuity), we recover the *nonlinear Kolmogorov n-width* defined in [29] as:

$$\delta_n(\mathcal{S}) := \inf_{\substack{E \in \mathcal{C}(\mathcal{S}, \mathbb{R}^n) \\ D \in \mathcal{C}(\mathbb{R}^n, X)}} \sup_{u \in \mathcal{S}} \|u - D(E(u))\|_X.$$

The smallest value of n such that perfect reconstruction is possible defines *the minimal latent dimension*:

$$n_\delta(\mathcal{S}) := \min \{n \in \mathbb{N} \mid \delta_n(\mathcal{S}) = 0\}. \quad (10)$$

In [33], the authors establish that for a solution manifold \mathcal{S} defined as the image of a *Lipschitz* parameter-to-solution map $u : \boldsymbol{\mu} \mapsto u(\boldsymbol{\mu})$, with a compact parameter set $\mathcal{P} \subset \mathbb{R}^p$, the minimal latent dimension satisfies:

$$p \leq n_\delta(\mathcal{S}) \leq 2p + 1. \quad (11)$$

Moreover, if the map $u : \mathcal{P} \rightarrow \mathcal{S}$ is *continuous and injective*, then it defines a homeomorphism between \mathcal{P} and \mathcal{S} , and in that case $n_\delta(\mathcal{S}) = p$ (see also [56]).

This framework provides a nonlinear generalization of the (linear) *Kolmogorov n-width*, see equation (3), where the decoder D is restricted to be linear and E is the orthogonal projection onto an n -dimensional subspace $\mathcal{V}_n \subset X$.

In this work, we are particularly interested in an intermediate notion between the fully linear and fully nonlinear frameworks, namely the *sensing numbers*. In this setting, the encoder is restricted to be linear—defined by n continuous linear forms of the dual space X' : $E = (\ell_1, \dots, \ell_n)$, while the decoder is allowed to be nonlinear. The corresponding width is defined as:

$$s_n(\mathcal{S}) := \inf_{\substack{D \in \mathcal{C}(\mathbb{R}^n, X) \\ \ell_1, \dots, \ell_n \in X'}} \sup_{u \in \mathcal{S}} \|u - D(\ell_1(u), \dots, \ell_n(u))\|_X. \quad (12)$$

This last notion retains the simplicity and interpretability of linear encoders, while benefiting from the expressive power of nonlinear decoders. As such, sensing numbers provide a promising compromise between classical linear approaches, governed by $d_n(\mathcal{S})$, and fully nonlinear reductions associated with $\delta_n(\mathcal{S})$.

By construction, the following inequalities hold:

$$\delta_n(\mathcal{S}) \leq s_n(\mathcal{S}) \leq d_n(\mathcal{S}), \quad (13)$$

which implies, for the associated minimal latent dimensions:

$$p \leq n_\delta(\mathcal{S}) \leq n_s(\mathcal{S}), \quad (14)$$

where $n_s(\mathcal{S})$ is defined as in equation (10) *mutatis mutandis*. However, unlike the case of $n_\delta(\mathcal{S})$ for which upper bounds are available (see equation (11)), no general upper bound is currently known for $n_s(\mathcal{S})$.

In [9], it was shown numerically for a specific test case that $n_s(\mathcal{S}) = p$ using a linear encoder based on projection onto SVD modes. In the present work, we rigorously establish that, at least **locally** and under suitable regularity assumptions, the minimal dimension satisfies $n_s(\mathcal{S}) = p$. This shows that the optimal encoding dimension is attainable with linear encoders in a neighborhood of the solution manifold.

3.2 Nonlinear Compressive Reduced Basis Approximation

The underlying idea in the NCRBA method is that, although the representation proposed by the linear approximation method (SVD, Greedy, GSS) to provide a good approximation is too large, it is nevertheless optimal in a certain sense. Based on this, the approximation consists of a sum

$$u(\boldsymbol{\mu}) \simeq u_N(\boldsymbol{\mu}) = \sum_{k=1}^N \alpha_k(\boldsymbol{\mu}) \varphi_k$$

where, in the “vanilla” version of the reduced basis method the coefficients $\alpha_k(\boldsymbol{\mu})$ for $k = 1, \dots, N$ are the solutions to a system of N equations derived by a Galerkin-type approximation associated with the PDE in equation (1) :

$$P_{\mathcal{V}_N}(\mathfrak{R}(u_N(\boldsymbol{\mu}); \boldsymbol{\mu})) = 0, \quad (15)$$

In the context where the complexity of \mathcal{S} , linked to the complexity of the set of parameters, is lower, the NCRBA suggests that only a few coefficients are true unknowns (degrees of freedom) and that the other coefficients necessary for the accuracy of the approximation are given functions of these degrees of freedom. More precisely, the first modes, from 1 to $n < N$, are the degrees of freedom, from which the remaining ones can be recovered. This means that we base our approach on a linear encoder (being the projection of the function on the first n reduced modes) and a nonlinear decoder that reads in a statement

$$\forall j = n+1, \dots, N, \quad \alpha_j(\boldsymbol{\mu}) = \psi^j(\alpha_1(\boldsymbol{\mu}), \alpha_2(\boldsymbol{\mu}), \dots, \alpha_n(\boldsymbol{\mu})),$$

where ψ^j are some feature maps that have to be suitably determined to represent well the large modes. This results in a problem of the form : Find $u_{\boldsymbol{\mu}}^{n,N}$ in \mathcal{V}_N that is written as

$$u_{\boldsymbol{\mu}}^{n,N} = \sum_{i=1}^n \alpha_{i,\boldsymbol{\mu}} \varphi_i + \sum_{j=n+1}^N \psi^j(\alpha_{1,\boldsymbol{\mu}}, \dots, \alpha_{n,\boldsymbol{\mu}}) \varphi_j, \quad (16)$$

such that

$$\Pi_n(\mathfrak{R}(u_{\boldsymbol{\mu}}^{n,N}; \boldsymbol{\mu})) = 0, \quad (17)$$

where Π_n is some rank n operator.

In this equation, the degrees of freedom are the n values $\{\alpha_{i,\boldsymbol{\mu}}\}_{i=1,\dots,n}$, and $\psi^j(\{\alpha_{i,\boldsymbol{\mu}}\}_{i=1,\dots,n})$ are the $j = n+1, \dots, N$ reduced basis coefficients, which are functions of the degrees of freedom. In our case, we choose a Galerkin approximation and choose Π_n to be the Galerkin projection on \mathcal{V}_n (an alternative, better choice could be obtained by minimizing the residual instead). Problem (16)-(17) being nonlinear, iterative methods are usually suited to solve it. Since we are considering small problems, we can use a Picard iteration procedure, as suggested below :

$$\sum_{i=1}^n \alpha_{i,\boldsymbol{\mu}}^{k+1} \varphi_i = \sum_{i=1}^n \alpha_{i,\boldsymbol{\mu}}^k \varphi_i - \gamma_k \Pi_n(\mathfrak{R}(u^k; \boldsymbol{\mu})), \quad (18)$$

where γ_k is a sequence of parameters indexed by k , and where we leave all dependencies in $\boldsymbol{\mu}, n$ and N , and

$$u^k = \sum_{i=1}^n \alpha_{i,\boldsymbol{\mu}}^k \varphi_i + \sum_{j=n+1}^N \psi^j(\{\alpha_{i,\boldsymbol{\mu}}^k\}_{i=1,\dots,n}) \varphi_j. \quad (19)$$

For a larger problem, a Newton or quasi-Newton method should be implemented. This important issue, both in terms of numerical efficiency and in terms of the error associated with the approximate solution, will be addressed in future work specifically devoted to it.

In what follows, we shall investigate different ways to express the ψ^j , $j = n+1, \dots, N$ as a function of the $\alpha_{i,\boldsymbol{\mu}}$, $j = 1, \dots, n$, together with the proper choice for $n \leq N$. This can be *i*) a quadratic expression, *i₁*) homogeneous (as in [10, 37, 62]), or *i₂*) non homogeneous, *ii*) a polynomial expression [35], or *iii*) finally a more general, learnable expression, as is proposed e.g. in [24, 11, 13, 26].

4 Approximation with Taylor polynomial expansions

In this section, we work in an abstract setting where $\mathcal{S} \subset X = \mathbb{R}^{\mathcal{M}}$ is an arbitrary embedded manifold. In particular, \mathcal{S} need not be associated with any parametrized PDE. In addition, the subsequent theory is developed independently of any discretization. This allows us to clarify the statements regardless of the properties of the map that to every parameter $\boldsymbol{\mu} \in \mathcal{P}$ associates the solution to the PDE. The purpose of this section is to show that the SVD analysis allows to determine the dimension q of the manifold \mathcal{S} and that there is a bijection between (i) the subspace spanned by the q first modes obtained from the SVD analysis of the elements sampled in the manifold \mathcal{S} and (ii) the tangent space to \mathcal{S} . In a vein similar to our contribution – though focused on a different application – this paper [65] offers particularly interesting insights.

A consequence of our analysis is that: locally, around each point on the manifold \mathcal{S} , the minimal dimension $n_s(\mathcal{S}) = q$. In particular, the approximation (16) is valid, asymptotically with $n = q$ and the functions ψ^j , for $j = q + 1, \dots, q + \frac{q(q+1)}{2}$ are (close to) quadratic in the q first coefficients. In addition, assuming that the manifold is of class \mathcal{C}^∞ , the approximation will improve by increasing the number of modes after the $q + \frac{q(q+1)}{2}$ first ones and increasing the degree of the polynomial approximation. Note, however, that this proof holds only asymptotically: for a wider variation of the parameters, we have to go beyond polynomial representation for the ψ^j , j larger than $n = q$.

Remark 2. Throughout this section, the matrix norm $\|\cdot\|$ stands for any sub-multiplicative and unitarily invariant norm. In particular, both the spectral norm $\|\cdot\|_2$ and the Frobenius norm $\|\cdot\|_F$ satisfy the required properties.

4.1 Notations and Assumptions

Consider a manifold \mathcal{S} of finite dimension q (the precise value of which is not known), embedded in $\mathbb{R}^{\mathcal{M}}$ (with dimension $\mathcal{M} \gg q$). Let \mathbf{u}^* be a point in this manifold; by definition, it serves as the support of a local map denoted as $U : \mathcal{Q}^0 \subset \mathbb{R}^q \longrightarrow \mathbb{R}^{\mathcal{M}}$ (the inverse of a chart) that locally parametrizes \mathcal{S} , with \mathcal{Q}^0 being an open subset of \mathbb{R}^q that contains, say, the ball $\mathcal{B}(\mathbf{0}, 1)$ in \mathbb{R}^q , centered at $\mathbf{0} \in \mathbb{R}^q$ with radius 1, and such that $U(\mathbf{0}) = \mathbf{u}^*$. There exists a real number $r^* > 0$ such that each point $\mathbf{u} \in \mathcal{S} \cap \mathcal{B}_{\mathbb{R}^{\mathcal{M}}}(\mathbf{u}^*, r^*)$ can be written as $\mathbf{u} = U(\boldsymbol{\nu})$ for some parameter $\boldsymbol{\nu} = (\nu_j)_{j=1}^q \in \mathcal{Q}^0$. We assume that the manifold is smooth enough (we need \mathcal{C}^3 in what follows) such that the Jacobian (resp. the second fundamental form associated to the Hessian) of U at every point in \mathcal{Q}^0 is non-singular (resp. has maximal rank) and spans a tangent space of dimension q (resp. a curvature space of dimension $\frac{1}{2}q(q+1)$).

To locally perform the singular value decomposition of the manifold \mathcal{S} , we first select a discrete dataset $\{\boldsymbol{\nu}^i\}_{i=1}^M \in \mathcal{B}(\mathbf{0}, 1)$, with M sufficiently large to provide a locally adequate sampling of U in \mathcal{Q}^0 , and thus a local sampling of \mathcal{S} around \mathbf{u}^* , with corresponding points $\{\mathbf{u}_i\}_{i=1}^M$, where for each i , $\mathbf{u}_i = U(\boldsymbol{\nu}^i)$. Next, for any r , $0 < r \leq r^*$, we consider the family of sampling of \mathcal{S} around \mathbf{u}^* , indexed by r , that converges to \mathbf{u}^* as $r \rightarrow 0$, defined by the set of discrete points $\{\mathbf{u}_i^r\}_{i=1}^M$, where for each i , $\mathbf{u}_i^r = U(r \cdot \boldsymbol{\nu}^i)$. This set of points can be considered as a sampling of $\mathcal{S}^r = \{U(\boldsymbol{\nu}), \boldsymbol{\nu} \in \mathcal{B}(\mathbf{0}, r) \subset \mathbb{R}^q\} \subset \mathcal{S}$. The values of M and r^* are not addressed in this discussion; refer to [65] for detailed information.

4.2 Tangent space of the centered manifold

For the sake of simplification, let us now “center” the manifold at \mathbf{u}^* and thus consider, for any given r , $0 < r \leq r^*$, the family of discrete points $\{\mathbf{v}_i^r = \mathbf{u}_i^r - \mathbf{u}^*\}_{i=1}^M$ on the shifted manifold $\mathcal{S}^{*,r} := \mathcal{S}^r - \mathbf{u}^* = \{\mathbf{v} = \mathbf{u} - \mathbf{u}^*, \mathbf{u} \in \mathcal{S}^r\} \subset \mathcal{S}^* := \mathcal{S} - \mathbf{u}^*$. The tangent space $T_0^* = T_0 \mathcal{S}^* = T_{\mathbf{u}^*} \mathcal{S}$ at the origin is the vector space spanned by the partial derivatives of the parameterization functions $U(\boldsymbol{\nu})$. Formally, we have:

$$T_0^* = \text{span} \left(\frac{\partial U}{\partial \nu_1}(\mathbf{0}), \frac{\partial U}{\partial \nu_2}(\mathbf{0}), \dots, \frac{\partial U}{\partial \nu_q}(\mathbf{0}) \right),$$

where the vectors $\frac{\partial U}{\partial \nu_j}(\mathbf{0})$ are the columns of the Jacobian matrix $\mathbf{J}_U(\boldsymbol{\nu}) \in \mathbb{R}^{\mathcal{M} \times q}$ (evaluated at $\boldsymbol{\nu} = \mathbf{0}$).

4.2.1 Convergence of the first order modes

As $r \rightarrow 0$, all points \mathbf{u}_i^r (resp. \mathbf{v}_i^r) become arbitrarily close to each other on the manifold \mathcal{S} (resp. \mathcal{S}^*) and converge to \mathbf{u}^* (resp. $\mathbf{0}$). At first-order, this gives, for any $i, 1 \leq i \leq M$:

$$\mathbf{v}_i^r = \mathbf{0} + r \sum_{j=1}^q \nu_j^i \frac{\partial U}{\partial \nu_j}(\mathbf{0}) + \mathcal{O}(r^2) \approx r \sum_{j=1}^q \nu_j^i \frac{\partial U}{\partial \nu_j}(\mathbf{0}),$$

as $r \rightarrow 0$.

Let $\mathbf{S}^r = [\mathbf{v}_1^r, \mathbf{v}_2^r, \dots, \mathbf{v}_M^r]$ be a snapshot matrix of $\mathcal{S}^{*,r}$. Using the above approximation for each \mathbf{v}_i^r , we have the following matrix approximation

$$\mathbf{S}^r = \mathbf{U}^r \boldsymbol{\Sigma}^r \mathbf{Z}^{r\top} = r \mathbf{A}_0 + \mathcal{O}(r^2), \quad \mathbf{A}_0 := \mathbf{J}_U(\mathbf{0}) \mathbf{P}, \quad (20)$$

where $\mathbf{P} = [\boldsymbol{\nu}^1, \boldsymbol{\nu}^2, \dots, \boldsymbol{\nu}^M]$ of size $q \times M$ and $\mathbf{J}_U(\mathbf{0})$ is the Jacobian of U at $\mathbf{0}$. By the assumption on the non-singularity of the Jacobian matrix, the rank of $\mathbf{J}_U(\mathbf{0})$ is equal to q . In addition, from the assumption made on the sampling of \mathcal{S} , the matrix \mathbf{P} also has rank q and consequently so does \mathbf{A}_0 . Therefore, for any small $r > 0$, from the matrix relation $\frac{1}{r} \mathbf{U}^r \boldsymbol{\Sigma}^r \mathbf{Z}^{r\top} \approx \mathbf{J}_U(\mathbf{0}) \mathbf{P}$ we deduce that (i) there is a clear gap in the size of the singular values present in $\boldsymbol{\Sigma}^r$ between the q^{th} and the $(q+1)^{th}$, which allows to determine the value of q if it is not known, (ii) from the theory of Davis-Kahan applied to the POD version of the SVD, the subspace $\mathcal{U}_{1:q}^r$ spanned by the first q left singular vectors of \mathbf{S}^r converges in $\mathcal{O}(r)$ to the tangent space T_0^* .

The formalization of this convergence of the distance between two subspaces (or associated generating vectors or matrices) involves the notion of *principal angles*, the definition of which is extensively recalled in Appendix A.

Theorem 1 (Convergence to the tangent space). *As $r \rightarrow 0$, the subspace $\mathcal{U}_{1:q}^r$ spanned by the first q left singular vectors of \mathbf{S}^r converges to the tangent space T_0^* with rate $\mathcal{O}(r)$, i.e.*

$$\|\sin \Theta(\mathcal{U}_{1:q}^r, T_0^*)\| = \mathcal{O}(r).$$

Proof. Let us define the scaled Gram matrices

$$\mathbf{C}_r := \frac{1}{r^2} \mathbf{S}^r (\mathbf{S}^r)^\top, \quad \mathbf{C}_0 := \mathbf{A}_0 \mathbf{A}_0^\top.$$

Then, from the first-order expansion (20), we derive

$$\mathbf{C}_r = (\mathbf{A}_0 + \mathcal{O}(r)) (\mathbf{A}_0 + \mathcal{O}(r))^\top = \mathbf{C}_0 + \mathcal{O}(r),$$

so that $\|\mathbf{C}_r - \mathbf{C}_0\| = \mathcal{O}(r)$. The matrix \mathbf{C}_0 has rank q , with q positive eigenvalues separated from 0 by a fixed spectral gap $\delta_q = \lambda_q(\mathbf{C}_0) > 0$ independent of r . Provided r is sufficiently small such that $\|\mathbf{C}_r - \mathbf{C}_0\| < \delta_q$, the Davis-Kahan $\sin \Theta$ theorem yields

$$\|\sin \Theta(\mathbf{U}_{(1)}^r, \mathbf{U}_{(1)}^*)\| \leq \frac{2\|\mathbf{C}_r - \mathbf{C}_0\|}{\delta_q} = \mathcal{O}(r),$$

where

$$\mathbf{U}_{(1)}^r := \mathbf{U}_{(:,1:q)}^r = [\boldsymbol{\varphi}_1^r, \dots, \boldsymbol{\varphi}_q^r], \quad \mathbf{U}_{(1)}^* := \mathbf{U}_{(:,1:q)}^* = [\boldsymbol{\varphi}_1^*, \dots, \boldsymbol{\varphi}_q^*], \quad (21)$$

and the columns $\boldsymbol{\varphi}_j^r$ and $\boldsymbol{\varphi}_j^*$ denote the first q left singular vectors of \mathbf{S}^r and of $\mathbf{J}_U(\mathbf{0}) \mathbf{P}$, respectively. Equivalently, they are the eigenvectors associated with the q largest eigenvalues of the Gram matrices \mathbf{C}_r and \mathbf{C}_0 . Since $\text{Range}(\mathbf{U}_{(1)}^r) = \mathcal{U}_{1:q}^r$ and $\text{Range}(\mathbf{U}_{(1)}^*) = T_0^*$, the claim follows. \square

However, the convergence of the individual SVD modes and thus the SVD basis is more delicate and not immediate: the (norm 1) singular vectors are not uniquely defined, one can only guarantee convergence up to an orthogonal transformation, i.e., for each sufficiently small $r > 0$, there exists an orthogonal matrix $\mathbf{O}_{(1)}^r \in O(q)$, where $O(q)$ stands for the orthogonal group, such that

$$\|\mathbf{U}_{(1)}^r - \mathbf{U}_{(1)}^* \mathbf{O}_{(1)}^r\| = \mathcal{O}(r). \quad (22)$$

The precise construction of $\mathbf{O}_{(1)}^r$ and the discussion of the role of simple versus multiple singular values are deferred to Appendix B.

4.2.2 Convergence of the coefficients

With the notations above, the “reduced basis” like approximation of $U(\boldsymbol{\nu})$ reads as follows

$$U(\boldsymbol{\nu}) \approx \mathbf{u}^* + \sum_{j=1}^q \alpha_j^r(\boldsymbol{\nu}) \varphi_j^r = \mathbf{u}^* + \mathbf{U}_{(1)}^r \boldsymbol{\alpha}_{(1)}^r(\boldsymbol{\nu}), \quad (23)$$

where

$$\boldsymbol{\alpha}_{(1)}^r(\boldsymbol{\nu}) := (\alpha_1^r(\boldsymbol{\nu}), \dots, \alpha_q^r(\boldsymbol{\nu})) = \mathbf{U}_{(1)}^{r\top} \mathbf{v}(\boldsymbol{\nu}), \quad (24)$$

is the coordinate vector of $\mathbf{v}(\boldsymbol{\nu})$ in the basis $\mathbf{U}_{(1)}^r$. We then introduce the projection coefficients onto the limiting tangent basis $\mathbf{U}_{1:q}^*$:

$$\boldsymbol{\alpha}_{(1)}^*(\boldsymbol{\nu}) := \mathbf{U}_{(1)}^{*\top} \mathbf{v}(\boldsymbol{\nu}). \quad (25)$$

From the assumed regularity on U , we observe that the first-order Taylor expansion is

$$U(\boldsymbol{\nu}) = \mathbf{u}^* + \sum_{j=1}^q \nu_j \frac{\partial U}{\partial \nu_j}(\mathbf{0}) + \mathcal{R}_2(\boldsymbol{\nu}) = \mathbf{u}^* + \mathbf{J}_U(\mathbf{0}) \boldsymbol{\nu} + \mathcal{R}_2(\boldsymbol{\nu}), \quad \|\mathcal{R}_2(\boldsymbol{\nu})\| = \mathcal{O}(\|\boldsymbol{\nu}\|^2). \quad (26)$$

Then, we express the (centered) Taylor expansion in the basis of the q SVD modes $\{\varphi_j^*\}_{j=1,\dots,q}$, there exist q linear forms β_j^* (expressing the change of basis set) in $\boldsymbol{\nu}$ such that

$$\sum_{j=1}^q \nu_j \frac{\partial U}{\partial \nu_j}(\mathbf{0}) = \sum_{j=1}^q \beta_j^*(\boldsymbol{\nu}) \varphi_j^*. \quad (27)$$

Let \mathbf{A}^* be the change-of-basis matrix between the tangent basis $\{\frac{\partial U}{\partial \nu_j}(\mathbf{0})\}_{j=1}^q$ and the orthonormal basis $\{\varphi_j^*\}_{j=1}^q$. From equation (27), one verifies that:

$$\mathbf{A}^* \boldsymbol{\nu} = \boldsymbol{\beta}_{(1)}^*(\boldsymbol{\nu}), \text{ and } \mathbf{A}^* = \mathbf{U}_{(1)}^{*\top} \mathbf{J}_U(\mathbf{0}), \quad (28)$$

where $\boldsymbol{\beta}_{(1)}^*(\boldsymbol{\nu}) := (\beta_1^*(\boldsymbol{\nu}), \dots, \beta_q^*(\boldsymbol{\nu}))$. In addition, the basis convergence result equation (22) implies:

$$\mathbf{U}_{(1)}^{r\top} = (\mathbf{O}_{(1)}^r)^\top \mathbf{U}_{(1)}^{*\top} + \mathbf{E}^r, \quad \|\mathbf{E}^r\| = \mathcal{O}(r). \quad (29)$$

We now state the result on the convergence of the coefficients.

Proposition 2 (Convergence of the coefficients). *For all $\boldsymbol{\nu} \in \mathcal{B}(\mathbf{0}, r)$, the coefficients $\boldsymbol{\alpha}_{(1)}^r(\boldsymbol{\nu})$ of the approximation of $U(\boldsymbol{\nu})$ in the basis $\mathbf{U}_{(1)}^r$ satisfy*

$$\boldsymbol{\alpha}_{(1)}^r(\boldsymbol{\nu}) = (\mathbf{O}_{(1)}^r)^\top \boldsymbol{\alpha}_{(1)}^*(\boldsymbol{\nu}) + \mathbf{e}_1^r = (\mathbf{O}_{(1)}^r)^\top \boldsymbol{\beta}_{(1)}^*(\boldsymbol{\nu}) + \mathbf{e}_1^r + \mathbf{e}_2^r = (\mathbf{O}_{(1)}^r)^\top \mathbf{A}^* \boldsymbol{\nu} + \mathbf{e}_1^r + \mathbf{e}_2^r, \quad (30)$$

where \mathbf{e}_1^r satisfies $\|\mathbf{e}_1^r\| = \mathcal{O}(r \|\boldsymbol{\nu}\|)$ and $\|\mathbf{e}_2^r\| = \mathcal{O}(\|\boldsymbol{\nu}\|^2)$. Reciprocally, we have

$$\boldsymbol{\nu} = \mathbf{B}^r \boldsymbol{\alpha}_{(1)}^r(\boldsymbol{\nu}) + \mathcal{O}(r \|\boldsymbol{\alpha}_{(1)}^r(\boldsymbol{\nu})\| + \|\boldsymbol{\alpha}_{(1)}^r(\boldsymbol{\nu})\|^2). \quad (31)$$

where $\mathbf{B}^r := (\mathbf{A}^*)^{-1} \mathbf{O}_{(1)}^r$.

The first equality in (30) shows that, as $r \rightarrow 0$, the empirical coefficients $\boldsymbol{\alpha}_{(1)}^r(\boldsymbol{\nu})$ converge to the projection coefficients $\boldsymbol{\alpha}_{(1)}^*(\boldsymbol{\nu})$ on the tangent space, both being nonlinear functions of $\boldsymbol{\nu}$. The second equality expresses that, in a Taylor sense, $\boldsymbol{\alpha}_{(1)}^r$ and $\boldsymbol{\beta}_{(1)}^*$ share the same first-order linear behavior up to $\mathcal{O}(\|\boldsymbol{\nu}\|^2)$, and in particular they are linear to order $\mathcal{O}(r^2)$ for $\boldsymbol{\nu} \in \mathcal{B}(\mathbf{0}, r)$.

Proof. From the definitions (24) of $\boldsymbol{\alpha}_{(1)}^r(\boldsymbol{\nu})$ and (25) of $\boldsymbol{\alpha}_{(1)}^*(\boldsymbol{\nu})$ together with the basis convergence (29), we obtain

$$\boldsymbol{\alpha}_{(1)}^r(\boldsymbol{\nu}) = (\mathbf{O}_{(1)}^r)^\top \mathbf{U}_{(1)}^{*\top} \mathbf{v}(\boldsymbol{\nu}) + \mathbf{e}_1^r(\boldsymbol{\nu}) = (\mathbf{O}_{(1)}^r)^\top \boldsymbol{\alpha}_{(1)}^*(\boldsymbol{\nu}) + \mathbf{e}_1^r(\boldsymbol{\nu}),$$

where $\mathbf{e}_1^r(\boldsymbol{\nu}) := \mathbf{E}^r \mathbf{v}(\boldsymbol{\nu})$. Since $\|\mathbf{E}^r\| = \mathcal{O}(r)$ and $\|\mathbf{v}(\boldsymbol{\nu})\| = \mathcal{O}(\|\boldsymbol{\nu}\|)$ that results from the regularity assumption on \mathbf{U} , we directly obtain the first equality.

Then, from the Taylor expansion in equation (26) we write

$$\boldsymbol{\alpha}_{(1)}^r(\boldsymbol{\nu}) = (\mathbf{O}_{(1)}^r)^\top \mathbf{U}_{(1)}^{*\top} (\mathbf{J}_U(\mathbf{0}) \boldsymbol{\nu} + \mathcal{R}_2(\boldsymbol{\nu})) + \mathbf{e}_1^r(\boldsymbol{\nu}) = (\mathbf{O}_{(1)}^r)^\top \boldsymbol{\beta}_{(1)}^*(\boldsymbol{\nu}) + \mathbf{e}_1^r(\boldsymbol{\nu}) + \mathbf{e}_2^r(\boldsymbol{\nu}),$$

with $\mathbf{e}_2^r(\boldsymbol{\nu}) := (\mathbf{O}_{(1)}^r)^\top \mathbf{U}_{(1)}^{*\top} \mathcal{R}_2(\boldsymbol{\nu})$, that, again from (26), satisfies the bound $\|\mathbf{e}_2^r(\boldsymbol{\nu})\| \leq c_2 \|\boldsymbol{\nu}\|^2 = \mathcal{O}(\|\boldsymbol{\nu}\|^2)$. and ends the proof of (30).

Next, from (28), we deduce that, uniformly on $\mathcal{B}(\mathbf{0}, r)$,

$$\boldsymbol{\alpha}_{(1)}^r(\boldsymbol{\nu}) = (\mathbf{O}_{(1)}^r)^\top \mathbf{A}^* \boldsymbol{\nu} + \mathcal{O}(r\|\boldsymbol{\nu}\| + \|\boldsymbol{\nu}\|^2),$$

hence

$$\boldsymbol{\nu} = \mathbf{B}^r \boldsymbol{\alpha}_{(1)}^r(\boldsymbol{\nu}) + \mathcal{O}(r\|\boldsymbol{\nu}\| + \|\boldsymbol{\nu}\|^2).$$

Using $\|\boldsymbol{\nu}\| = \mathcal{O}(\|\boldsymbol{\alpha}_{(1)}^r(\boldsymbol{\nu})\|)$ on $\mathcal{B}(\mathbf{0}, r)$ (uniform invertibility of the Jacobian, see Lemma 3), we obtain (31). \square

4.2.3 Local invertibility of the coefficient map

In Section 4.2.2, we have seen that the first q coefficients $\boldsymbol{\alpha}_{(1)}^r(\boldsymbol{\nu})$ of the approximation of $U(\boldsymbol{\nu})$ in the SVD basis $\mathbf{U}_{(1)}^r$ are certainly functions of $\boldsymbol{\nu}$, whose expression has no reason to be simple, however, they behave linearly in $\boldsymbol{\nu}$ in the asymptotic regime $r \rightarrow 0$. In this section, we go further and establish a local bijection between these coefficients and the parameter $\boldsymbol{\nu}$. In other words, the mapping $\boldsymbol{\nu} \mapsto \boldsymbol{\alpha}_{(1)}^r(\boldsymbol{\nu})$ is locally invertible.

Lemma 3. *Let $\boldsymbol{\alpha}_{(1)}^r : \mathcal{B}(\mathbf{0}, r) \rightarrow \mathbb{R}^q$ be the coefficients of the approximation of $U(\boldsymbol{\nu})$ in the SVD basis $\mathbf{U}_{(1)}^r$ defined in (24), then $\boldsymbol{\alpha}_{(1)}^r$ is differentiable and, for $r > 0$ sufficiently small, its Jacobian $\mathbf{J}_{\boldsymbol{\alpha}_{(1)}^r}(\boldsymbol{\nu})$ is invertible at every point $\boldsymbol{\nu}$ of the ball $\mathcal{B}(\mathbf{0}, r)$ and there exists $K > 0$ such that:*

$$\sup_{\|\boldsymbol{\nu}\| \leq r} \|(\mathbf{J}_{\boldsymbol{\alpha}_{(1)}^r}(\boldsymbol{\nu}))^{-1}\| \leq K.$$

Proof. For any $j = 1, \dots, q$, the gradient of $\alpha_j^r(\boldsymbol{\nu})$ is given by:

$$\nabla_{\boldsymbol{\nu}} \alpha_j^r(\boldsymbol{\nu}) = \nabla_{\boldsymbol{\nu}} \left(\langle U(\boldsymbol{\nu}) - \mathbf{u}^*, \boldsymbol{\varphi}_j^r \rangle \right) = \mathbf{J}_U(\boldsymbol{\nu})^\top \boldsymbol{\varphi}_j^r.$$

Hence, the Jacobian matrix of $\boldsymbol{\alpha}_{(1)}^r$ at $\boldsymbol{\nu}$ reads:

$$\mathbf{J}_{\boldsymbol{\alpha}_{(1)}^r}(\boldsymbol{\nu}) = \begin{bmatrix} \nabla_{\boldsymbol{\nu}} \alpha_1^r(\boldsymbol{\nu})^\top \\ \vdots \\ \nabla_{\boldsymbol{\nu}} \alpha_q^r(\boldsymbol{\nu})^\top \end{bmatrix} = \mathbf{U}_{(1)}^{r\top} \mathbf{J}_U(\boldsymbol{\nu}).$$

Defining $\mathbf{A}_r^* := (\mathbf{O}_{(1)}^r)^\top \mathbf{A}^*$, which, like the change of basis \mathbf{A}^* , is invertible, and using the basis convergence result (29), we have:

$$\mathbf{J}_{\boldsymbol{\alpha}_{(1)}^r}(\boldsymbol{\nu}) - \mathbf{A}_r^* = \mathbf{U}_{(1)}^{r\top} (\mathbf{J}_U(\boldsymbol{\nu}) - \mathbf{J}_U(\mathbf{0})) + \mathbf{E}^r \mathbf{J}_U(\mathbf{0}).$$

Taking the supremum over $\|\boldsymbol{\nu}\| \leq r$, for any unitarily invariant norm we obtain

$$\sup_{\|\boldsymbol{\nu}\| \leq r} \|\mathbf{J}_{\boldsymbol{\alpha}_{(1)}^r}(\boldsymbol{\nu}) - \mathbf{A}_r^*\| \leq \omega_1(r) + C_1 r,$$

where $\omega_1(r) := \sup_{\|\boldsymbol{\nu}\| \leq r} \|\mathbf{J}_U(\boldsymbol{\nu}) - \mathbf{J}_U(\mathbf{0})\| \rightarrow 0$ as $r \rightarrow 0$ by continuity of \mathbf{J}_U at $\mathbf{0}$, and $C_1 > 0$ is independent of r . Choose $r > 0$ sufficiently small so that

$$\theta_r := \|(\mathbf{A}_r^*)^{-1}\| \sup_{\|\boldsymbol{\nu}\| \leq r} \|\mathbf{J}_{\boldsymbol{\alpha}_{(1)}^r}(\boldsymbol{\nu}) - \mathbf{A}_r^*\| \leq \|(\mathbf{A}^*)^{-1}\| (\omega_1(r) + C_1 r) < 1,$$

then $\mathbf{I} + (\mathbf{A}_r^*)^{-1}(\mathbf{J}_{\alpha_{(1)}^r}(\boldsymbol{\nu}) - \mathbf{A}_r^*) = (\mathbf{A}_r^*)^{-1}\mathbf{J}_{\alpha_{(1)}^r}$ reads as a perturbation of identity that is invertible with an inverse that can be written as a convergent Neumann series with norm upper bounded by $(1 - \theta_r)^{-1}$.

For every $\boldsymbol{\nu} \in \mathcal{B}(\mathbf{0}, r)$,

$$\mathbf{J}_{\alpha_{(1)}^r}(\boldsymbol{\nu}) = \mathbf{A}_r^* \left(\mathbf{I} + (\mathbf{A}_r^*)^{-1}(\mathbf{J}_{\alpha_{(1)}^r}(\boldsymbol{\nu}) - \mathbf{A}_r^*) \right)$$

is thus invertible and satisfies the following uniform bound

$$\|(\mathbf{J}_{\alpha_{(1)}^r}(\boldsymbol{\nu}))^{-1}\| = \left\| \left(\mathbf{I} + (\mathbf{A}_r^*)^{-1}(\mathbf{J}_{\alpha_{(1)}^r}(\boldsymbol{\nu}) - \mathbf{A}_r^*) \right)^{-1} \right\| \|(\mathbf{A}_r^*)^{-1}\| \leq (1 - \theta_r)^{-1} \|(\mathbf{A}_r^*)^{-1}\|.$$

Since $\|(\mathbf{A}_r^*)^{-1}\| = \|(\mathbf{A}^*)^{-1}\|$ (unitarily invariance) and, for r small enough, $\theta_r < \frac{1}{2}$, we obtain the explicit uniform estimate, valid for all $\boldsymbol{\nu} \in \mathcal{B}(\mathbf{0}, r)$:

$$\|(\mathbf{J}_{\alpha_{(1)}^r}(\boldsymbol{\nu}))^{-1}\| \leq (1 - \theta_r)^{-1} \|(\mathbf{A}^*)^{-1}\| \leq 2 \|(\mathbf{A}^*)^{-1}\|,$$

which ends the proof by setting $K := 2 \|(\mathbf{A}^*)^{-1}\|$. \square

At this level we can state that, for any r small enough, there exists $r' > 0$, with $r' \leq r$ such that the map $\alpha_{(1)}^r$ is a C^k -diffeomorphism from $\mathcal{B}(\mathbf{0}, r')$ onto its image. In order to prove that the results remain true for $r' = r$, we need some global property, i.e., prove that

Lemma 4. *There exists $r_0 > 0$ such that for all $0 < r < r_0$, the map $\alpha_{(1)}^r : \mathcal{B}(\mathbf{0}, r) \rightarrow \mathbb{R}^q$ is injective.*

Proof. From Lemma 3 and the continuity of $\mathbf{J}_{\alpha_{(1)}^r}$ at $\mathbf{0}$ we deduce that there exists $r_0 > 0$ small enough such that

$$\forall r, 0 < r \leq r_0, \quad \sup_{\|\boldsymbol{\nu}\| \leq r} \|(\mathbf{J}_{\alpha_{(1)}^r}(\boldsymbol{\nu}))^{-1}\| \leq K \quad \text{and} \quad \omega_2(r) := \sup_{\boldsymbol{\nu}_1, \boldsymbol{\nu}_2 \in \mathcal{B}(\mathbf{0}, r)} \|\mathbf{J}_{\alpha_{(1)}^r}(\boldsymbol{\nu}_1) - \mathbf{J}_{\alpha_{(1)}^r}(\boldsymbol{\nu}_2)\| \leq \frac{1}{2K}.$$

Let $\boldsymbol{\nu}_1, \boldsymbol{\nu}_2 \in \mathcal{B}(\mathbf{0}, r)$ and set $h := \boldsymbol{\nu}_1 - \boldsymbol{\nu}_2$, $\gamma(t) := \boldsymbol{\nu}_2 + th$ ($t \in [0, 1]$). By the fundamental theorem of calculus and the chain rule,

$$\alpha_{(1)}^r(\boldsymbol{\nu}_1) - \alpha_{(1)}^r(\boldsymbol{\nu}_2) = \int_0^1 \mathbf{J}_{\alpha_{(1)}^r}(\gamma(t)) h \, dt = \mathbf{J}_{\alpha_{(1)}^r}(\boldsymbol{\nu}_2) h + \int_0^1 (\mathbf{J}_{\alpha_{(1)}^r}(\gamma(t)) - \mathbf{J}_{\alpha_{(1)}^r}(\boldsymbol{\nu}_2)) h \, dt.$$

Taking norms and using the reverse triangle inequality yields

$$\|\alpha_{(1)}^r(\boldsymbol{\nu}_1) - \alpha_{(1)}^r(\boldsymbol{\nu}_2)\| \geq \|\mathbf{J}_{\alpha_{(1)}^r}(\boldsymbol{\nu}_2)h\| - \int_0^1 \|\mathbf{J}_{\alpha_{(1)}^r}(\gamma(t)) - \mathbf{J}_{\alpha_{(1)}^r}(\boldsymbol{\nu}_2)\| \|h\| \, dt.$$

By the uniform inverse bound, $\|\mathbf{J}_{\alpha_{(1)}^r}(\boldsymbol{\nu}_2)h\| \geq K^{-1}\|h\|$; by the definition of $\omega_2(r)$, the integral term is at most $\omega_2(r)\|h\|$. Hence

$$\|\alpha_{(1)}^r(\boldsymbol{\nu}_1) - \alpha_{(1)}^r(\boldsymbol{\nu}_2)\| \geq (K^{-1} - \omega_2(r)) \|h\|.$$

With $\omega_2(r) \leq \frac{1}{2K}$, we get

$$\|\alpha_{(1)}^r(\boldsymbol{\nu}_1) - \alpha_{(1)}^r(\boldsymbol{\nu}_2)\| \geq \frac{1}{2K} \|\boldsymbol{\nu}_1 - \boldsymbol{\nu}_2\|.$$

Therefore $\alpha_{(1)}^r(\boldsymbol{\nu}_1) = \alpha_{(1)}^r(\boldsymbol{\nu}_2)$ implies $\boldsymbol{\nu}_1 = \boldsymbol{\nu}_2$, i.e., $\alpha_{(1)}^r$ is injective on $\mathcal{B}(\mathbf{0}, r)$. \square

Proposition 5 (C^k -diffeomorphism on a neighborhood of the ball). *Assume U is of class C^k on a neighborhood A of $\mathbf{0}$ for some k , $1 \leq k \leq \infty$, then there exists $r_0 > 0$ such that, for every $0 < r < r_0$, the map $\alpha_{(1)}^r$ is a C^k -diffeomorphism from $\mathcal{B}(\mathbf{0}, r)$ onto its image $\alpha_{(1)}^r(\mathcal{B}(\mathbf{0}, r)) \subset \mathbb{R}^q$.*

Proof. Each component $\alpha_j^r(\boldsymbol{\nu}) = \langle U(\boldsymbol{\nu}) - \mathbf{u}^*, \varphi_j^r \rangle$ is the composition of $U \in C^k(A; \mathbb{R}^M)$ with a bounded linear functional, hence $\alpha_j^r \in C^k(A; \mathbb{R}^q)$. There exists $r_0 > 0$, small enough such that, for any $r \leq r_0$,

- by Lemma 3, the Jacobian $\mathbf{J}_{\alpha_{(1)}^r}(\boldsymbol{\nu})$ is invertible on $\mathcal{B}(\mathbf{0}, r)$ with uniformly bounded inverse,
- by Lemma 4, $\alpha_{(1)}^r$ is injective on $\mathcal{B}(\mathbf{0}, r)$.

Applying the global inverse function theorem, we obtain that, for such values of $r \leq r_0$, we have $\alpha_{(1)}^r$ is a C^k -diffeomorphism from $\mathcal{B}(\mathbf{0}, r)$ onto its image. \square

4.2.4 Sensing numbers

The above proposition implies all the information on the elements $U(\boldsymbol{\nu})$ in the manifold \mathcal{S} , close enough to \mathbf{u}^* is present in the q first coefficients of its SVD decomposition, since we can recover $\boldsymbol{\nu}$ from $\boldsymbol{\alpha}_{(1)}^r(\boldsymbol{\nu})$.

From the perspective of sensing numbers (12), this will translate into the conclusion that the minimal latent dimension, at least locally, satisfies $n_s(\mathcal{S}^r) = q$. This property is particularly relevant in the context of parametric PDEs and the NCRBA, since it establishes the validity of the reduced approximation (16), and that all the information is contained locally in the first $n = q (= p)$ coefficients.

Proposition 6 (Centered manifold: local latent dimension). *The centered manifold \mathcal{S}^* has locally a latent (sensing) dimension equal to q around \mathbf{u}^* , i.e., for sufficiently small $r > 0$,*

$$n_s(\mathcal{S}^{*,r}) = q.$$

Proof. For $r > 0$ small enough, let $E : \mathbb{R}^{\mathcal{M}} \rightarrow \mathbb{R}^q$ be the linear encoder given by the projection onto the first q SVD modes of the centered snapshot matrix \mathbf{S}^r :

$$E : \mathbf{x} \mapsto \mathbf{U}_{(1)}^{r\top} \mathbf{x}.$$

The continuity of E is immediate, since it is an orthogonal projection operator. Now let $K^r := E(\mathcal{S}^{*,r}) = \boldsymbol{\alpha}_{(1)}^r(\mathcal{B}(\mathbf{0}, r))$, which is a compact subset of \mathbb{R}^q . By Proposition 5, the coefficient map

$$\boldsymbol{\alpha}_{(1)}^r : \mathcal{B}(\mathbf{0}, r) \rightarrow K^r$$

is a C^k -diffeomorphism. We then define the restriction of the decoder D on K^r as

$$D|_{K^r} : K^r \longrightarrow \mathbb{R}^{\mathcal{M}}, \quad D|_{K^r} := \mathbf{v} \circ (\boldsymbol{\alpha}_{(1)}^r)^{-1},$$

where $\mathbf{v} = U - \mathbf{u}^*$. One can further define a continuous decoder on the whole space \mathbb{R}^q by continuously extending $D|_{K^r}$ to \mathbb{R}^q , this is guaranteed by the Tietze extension theorem. Then, for all $\boldsymbol{\nu} \in \mathcal{B}(\mathbf{0}, r)$,

$$(D \circ E)(\mathbf{v}(\boldsymbol{\nu})) = \mathbf{v}((\boldsymbol{\alpha}_{(1)}^r)^{-1}(\boldsymbol{\alpha}_{(1)}^r(\boldsymbol{\nu}))) = \mathbf{v}(\boldsymbol{\nu}).$$

Using this couple of Encoder-Decoder the reconstruction error in equation (9) is zero with $n = q$, so $n_s(\mathcal{S}^{*,r}) \leq q$. Conversely, from equation (14) $n_s(\mathcal{S}^{*,r}) \geq q$. We conclude $n_s(\mathcal{S}^{*,r}) = q$. \square

Lemma 7 (Translation invariance of sensing numbers). *For any $\mathbf{a} \in X$ and any $\mathcal{S} \subset X$,*

$$n_s(\mathcal{S} + \mathbf{a}) = n_s(\mathcal{S}).$$

Proof. We first show that for each $n \in \mathbb{N}$,

$$s_n(\mathcal{S} + \mathbf{a}) = s_n(\mathcal{S}). \quad (32)$$

For any fixed $\varepsilon > 0$, by definition of s_n we can choose an encoder-decoder pair $(E_\varepsilon, D_\varepsilon)$ with $E_\varepsilon : X \rightarrow \mathbb{R}^n$ linear and $D_\varepsilon \in \mathcal{C}(\mathbb{R}^n, X)$ such that

$$\sup_{\mathbf{u} \in \mathcal{S}} \|\mathbf{u} - D_\varepsilon(E_\varepsilon(\mathbf{u}))\|_X \leq s_n(\mathcal{S}) + \varepsilon.$$

Define a decoder $D_{\mathbf{a}, \varepsilon} : \mathbb{R}^n \rightarrow X$ by

$$D_{\mathbf{a}, \varepsilon}(\mathbf{x}) := \mathbf{a} + D_\varepsilon(\mathbf{x} - E_\varepsilon(\mathbf{a})),$$

and keep the same linear encoder E_ε . For any $\mathbf{v} \in \mathcal{S} + \mathbf{a}$ we can write $\mathbf{v} = \mathbf{u} + \mathbf{a}$ with $\mathbf{u} \in \mathcal{S}$, and then

$$D_{\mathbf{a}, \varepsilon}(E_\varepsilon(\mathbf{v})) = \mathbf{a} + D_\varepsilon(E_\varepsilon(\mathbf{u} + \mathbf{a}) - E_\varepsilon(\mathbf{a})) = \mathbf{a} + D_\varepsilon(E_\varepsilon(\mathbf{u})).$$

Hence

$$\|\mathbf{v} - D_{\mathbf{a}, \varepsilon}(E_\varepsilon(\mathbf{v}))\|_X = \|\mathbf{u} + \mathbf{a} - (\mathbf{a} + D_\varepsilon(E_\varepsilon(\mathbf{u})))\|_X = \|\mathbf{u} - D_\varepsilon(E_\varepsilon(\mathbf{u}))\|_X.$$

Taking the supremum over $\mathbf{v} \in \mathcal{S} + \mathbf{a}$ (equivalently $\mathbf{u} \in \mathcal{S}$) gives

$$\sup_{\mathbf{v} \in \mathcal{S} + \mathbf{a}} \|\mathbf{v} - D_{\mathbf{a}, \varepsilon}(E_\varepsilon(\mathbf{v}))\|_X = \sup_{\mathbf{u} \in \mathcal{S}} \|\mathbf{u} - D_\varepsilon(E_\varepsilon(\mathbf{u}))\|_X \leq s_n(\mathcal{S}) + \varepsilon,$$

so $s_n(\mathcal{S} + \mathbf{a}) \leq s_n(\mathcal{S}) + \varepsilon$. As $\varepsilon > 0$ is arbitrary, $s_n(\mathcal{S} + \mathbf{a}) \leq s_n(\mathcal{S})$.

Applying the same argument with translation by $-\mathbf{a}$ yields $s_n(\mathcal{S}) \leq s_n(\mathcal{S} + \mathbf{a})$. Therefore equation (32) holds.

Finally, by definition $n_s(\mathcal{S}) = \min\{n : s_n(\mathcal{S}) = 0\}$. Using equation (32), we conclude $n_s(\mathcal{S} + \mathbf{a}) = n_s(\mathcal{S})$. \square

Corollary 8 (Non-centered manifold: local latent dimension). *For sufficiently small $r > 0$,*

$$n_s(\mathcal{S}^r) = q.$$

Proof. By Proposition 6, $n_s(\mathcal{S}^{*,r}) = q$. Since $\mathcal{S}^r = \mathbf{u}^* + \mathcal{S}^{*,r}$, the translation invariance Lemma 7 yields

$$n_s(\mathcal{S}^r) = n_s(\mathbf{u}^* + \mathcal{S}^{*,r}) = n_s(\mathcal{S}^{*,r}) = q.$$

\square

Remark 3. 1. **Non-continuity of n_s .** The local result established in Corollary 8 cannot, in general, be extended to the whole manifold \mathcal{S} by a mere continuity argument, since n_s takes discrete values and would therefore have to remain constant on each connected component of \mathcal{S} .

For instance, in [29] it was shown that for the manifold

$$\mathcal{S} = \{\mathbf{x} \in \mathbb{R}^2 : \|\mathbf{x}\| = 1\},$$

i.e. the unit circle in $X = \mathbb{R}^2$, one has $n_\delta(\mathcal{S}) = 2 = q + 1$. In this example, Corollary 8 gives $n_s(\mathcal{S}^r) = q = 1$ locally, while globally

$$n_s(\mathcal{S}) \geq n_\delta(\mathcal{S}) = 2.$$

Hence, n_s is not continuous in general.

2. **Injectivity and sensing numbers.** Unlike for n_δ , the injectivity of the solution map is not sufficient to get $n_s = q$. Consider, for instance, the open arc of the unit circle

$$\mathcal{S} = \{ \mathbf{u}(\theta) = (\cos \theta, \sin \theta) : \theta \in (-\frac{3\pi}{4}, \frac{3\pi}{4}) \} \subset \mathbb{R}^2.$$

The mapping $\theta \mapsto \mathbf{u}(\theta)$ is injective, and the manifold \mathcal{S} is smooth and one-dimensional. However, there exists no nonzero linear form $\ell(x) = a^\top x$ such that ℓ restricted to \mathcal{S} remains injective. Indeed, for any direction $a = (\cos \varphi, \sin \varphi)$,

$$(\ell \circ \mathbf{u})(\theta) = \cos(\theta - \varphi),$$

which is not injective on any interval of length greater than π . Hence, even though \mathcal{S} is parametrized injectively by θ , no one-dimensional linear projection can preserve this injectivity, and consequently, the sensing number satisfies

$$n_s(\mathcal{S}) > 1.$$

3. **Non-centered case:** Even though we proved that locally around $\mathbf{u}^* \in \mathcal{S}$ one has $n_s(\mathcal{S}^r) = q$, the situation differs from the centered case (i.e. working on $\mathcal{S}^{*,r} = \mathcal{S}^r - \mathbf{u}^*$). In the non-centered setting, the first q SVD modes of the snapshot matrix are not necessarily aligned with the tangent space at \mathbf{u}^* , and therefore do not guarantee a bijection between the coefficients and the parameters ν . In fact, one additional mode (for a total of $q + 1$) may be required even locally: the first singular mode converges to the direction of \mathbf{u}^* itself, while the next q modes, along with \mathbf{u}^* , allow us to generate the tangent affine space.

4. **Conclusion:** From points 1 and 3 above, one can conclude that in either the non-local or the non-centered setting, at least $q + 1$ SVD modes may be necessary to recover the full information carried by the manifold, i.e., the full parameter value ν .

4.3 Second order Taylor expansion of the centered manifold

In this section, we extend the first-order analysis of the local manifold representation in section 4.2 to include second-order effects. Our goal is to characterize how the second-order empirical SVD modes and their associated projection coefficients behave. This higher-order analysis reveals the emergence of the curvature subspace in the SVD structure and a corresponding quadratic dependence in the reduced coordinates.

4.3.1 Convergence of the filtered second-order SVD modes

Under regularity assumptions on U , we can extend equation (20) to second order as:

$$\mathbf{S}^r = r \mathbf{A}_0 + \frac{r^2}{2} \mathbf{Q}_0 + \mathcal{O}(r^3). \quad (33)$$

Let $\mathcal{I} := \{(j, \ell) : 1 \leq j \leq \ell \leq q\}$ and $m := |\mathcal{I}| = \frac{q(q+1)}{2}$. Define the quadratic feature matrix $\mathbf{P}_2 \in \mathbb{R}^{m \times M}$ by

$$\mathbf{P}_2 := \left[\text{vec}_{\text{sym}}(\boldsymbol{\nu}^1 \boldsymbol{\nu}^{1\top}), \dots, \text{vec}_{\text{sym}}(\boldsymbol{\nu}^j \boldsymbol{\nu}^{j\top}), \dots, \text{vec}_{\text{sym}}(\boldsymbol{\nu}^M \boldsymbol{\nu}^{M\top}) \right],$$

where, for any symmetric matrix $\mathbf{A} = (a_{ij})$ of size q , $\text{vec}_{\text{sym}}(\mathbf{A})$ denotes the vector of size $m = \frac{q(q+1)}{2}$ containing the upper triangular part of \mathbf{A} row by row, i.e. $\text{vec}_{\text{sym}}(\mathbf{A}) := (a_{11}, a_{12}, \dots, a_{1q}, a_{22}, \dots, a_{2q}, \dots, a_{qq})^T$.

Define the (symmetrized) quadratic Taylor basis matrix $\mathbf{Q}_{\text{base}} \in \mathbb{R}^{M \times m}$ by

$$\mathbf{Q}_{\text{base}} := \left[(2 - \delta_{j\ell}) \partial_{\nu_j} \partial_{\nu_\ell} U(\mathbf{0}) \right]_{(j, \ell) \in \mathcal{I}},$$

with the same column ordering as $\text{vec}_{\text{sym}}(\cdot)$. Finally, define

$$\mathbf{Q}_0 := \mathbf{Q}_{\text{base}} \mathbf{P}_2 \in \mathbb{R}^{M \times M}.$$

Equivalently, the i -th column of \mathbf{Q}_0 , $i = 1, \dots, M$, is $D^2 U(\mathbf{0})[\boldsymbol{\nu}^i, \boldsymbol{\nu}^i]$.

Here, we focus on the second block of left singular vectors of \mathbf{S}^r , which captures the curvature effects of the manifold beyond the first SVD order. To isolate this second-order behavior, we perform the analysis on a projected snapshot matrix $\widehat{\mathbf{S}}^r := (\mathbf{I} - \Pi_0) \mathbf{S}^r$, where $\Pi_0 = \mathbf{U}_{(1)}^* \mathbf{U}_{(1)}^{*\top}$ is the orthogonal projection onto the tangent space. Since $(\mathbf{I} - \Pi_0) \mathbf{J}_U(0) = 0$, left-multiplying equation (33) by $(\mathbf{I} - \Pi_0)$ cancels the linear term (remember the definition of \mathbf{A}_0 in (20)):

$$\widehat{\mathbf{S}}^r = (\mathbf{I} - \Pi_0) \mathbf{S}^r = \frac{r^2}{2} (\mathbf{I} - \Pi_0) \mathbf{Q}_0 + \mathcal{O}(r^3) = \frac{r^2}{2} (\mathbf{I} - \Pi_0) \mathbf{Q}_{\text{base}} \mathbf{P}_2 + \mathcal{O}(r^3).$$

By the assumption on the second fundamental form associated with the Hessian matrix, $(\mathbf{I} - \Pi_0) \mathbf{Q}_{\text{base}}$ has (full) rank m . We further assume that the sampling is *quadratically rich* in the sense that $\text{rank}(\mathbf{P}_2) = m$ (in particular $M \geq m$), so that $\text{Range}((\mathbf{I} - \Pi_0) \mathbf{Q}_0) = \text{Range}((\mathbf{I} - \Pi_0) \mathbf{Q}_{\text{base}})$. Next, we define

$$\widehat{\mathbf{U}}_{(2)}^r := \left[\widehat{\boldsymbol{\varphi}}_1^r, \dots, \widehat{\boldsymbol{\varphi}}_m^r \right], \quad \mathbf{U}_{(2)}^* := \left[\boldsymbol{\varphi}_{q+1}^*, \dots, \boldsymbol{\varphi}_{q+m}^* \right], \quad (34)$$

where $\{\widehat{\boldsymbol{\varphi}}_j^r\}_{j=1}^m$ and $\{\boldsymbol{\varphi}_{q+j}^*\}_{j=1}^m$ denote the first m singular vectors of $\widehat{\mathbf{S}}^r$ and of $(\mathbf{I} - \Pi_0) \mathbf{Q}_0$, respectively. The basis $\mathbf{U}_{(2)}^* \in \mathbb{R}^{M \times m}$ spans the curvature subspace associated with the second-order variations of the manifold, defined as

$$\mathcal{C} := \text{span} \left\{ (\mathbf{I} - \Pi_0) \partial_{\nu_j} \partial_{\nu_\ell} U(\mathbf{0}) : 1 \leq j \leq \ell \leq q \right\} = \text{Range}(\mathbf{U}_{(2)}^*). \quad (35)$$

Theorem 9 (filtered curvature block converges to the curvature subspace). *As $r \rightarrow 0$, the subspace $\widehat{\mathcal{U}}_{1:m}^{r(2)}$ spanned by the m first left singular vectors of $\widehat{\mathbf{S}}^r$ converges to the curvature subspace \mathcal{C} with rate $\mathcal{O}(r)$, i.e.*

$$\| \sin \Theta(\widehat{\mathcal{U}}_{1:m}^{r(2)}, \mathcal{C}) \| = \mathcal{O}(r). \quad (36)$$

Proof. The scaled Gram matrices are given by

$$\widehat{\mathbf{C}}^r := r^{-4} \widehat{\mathbf{S}}^r \widehat{\mathbf{S}}^{r\top}, \quad \mathbf{C}_0 := \frac{1}{4} (\mathbf{I} - \Pi_0) \mathbf{Q}_0 \mathbf{Q}_0^\top (\mathbf{I} - \Pi_0),$$

and verify $\|\widehat{\mathbf{C}}^r - \mathbf{C}_0\|_2 = \mathcal{O}(r)$. The matrix \mathbf{C}_0 has rank m , with m positive eigenvalues separated from 0 by a fixed spectral gap $\delta_m = \lambda_m(\mathbf{C}_0) > 0$ independent of r . Provided r is sufficiently small, then $\|\widehat{\mathbf{C}}^r - \mathbf{C}_0\| < \delta_m$ and the Davis–Kahan sin Θ theorem (see Appendix p. 32) yields

$$\|\sin \Theta(\widehat{\mathcal{U}}_{1:m}^{r(2)}, \mathcal{C})\| \leq \frac{2\|\widehat{\mathbf{C}}^r - \mathbf{C}_0\|}{\delta_m} = \mathcal{O}(r),$$

where $\widehat{\mathcal{U}}_{1:m}^{r(2)} = \text{Range}(\widehat{\mathbf{U}}_{(2)}^r)$. \square

Remark 4 (Unfiltered curvature block). A natural question is whether the same $\mathcal{O}(r)$ convergence holds for the *unfiltered* second block of left singular vectors $\mathbf{U}_{(2)}^r$ defined by

$$\mathbf{U}_{(2)}^r := [\boldsymbol{\varphi}_{q+1}^r, \dots, \boldsymbol{\varphi}_{q+m}^r], \quad (37)$$

where the columns $\{\boldsymbol{\varphi}_{q+j}^r\}_{j=1}^m$ denote the second set of m left singular vectors of \mathbf{S}^r , without first projecting out the tangent space. This requires a more delicate analysis involving alignment matrices and careful tracking of cross-terms. However, numerical experiments suggest that the same $\mathcal{O}(r)$ convergence rate holds in practice for $\mathbf{U}_{(2)}^r$ as well, see section 6.3.

4.3.2 Quadratic law for the limit curvature frame coefficients

Having established the convergence of the second-order SVD modes $\widehat{\mathbf{U}}_{(2)}^r$ to the curvature subspace \mathcal{C} in the previous section, we now turn to a fundamental question: *what is the functional dependence of the curvature coefficients on the tangent coefficients?*

This question is central to nonlinear model reduction methods such as NCRBA (see section 3.2) and quadratic-manifold ROMs [10, 62, 37], which postulate that higher-order coefficients can be expressed as polynomial functions of the leading reduced coordinates.

Specifically, we show that the projection coefficients onto the curvature subspace — corresponding to SVD modes $q+1$ through $q+m$ — are quadratic in the tangent coefficients up to higher-order terms.

We first consider the limit case, which is independent of r . In Section 4.3.3, we then extend the result to the filtered case.

Theorem 10 (Quadratic law for the limit curvature frame block). *Let $\mathbf{U}_{(2)}^* \in \mathbb{R}^{\mathcal{M} \times m}$ defined in (34) be $\mathbf{U}_{(2)}^* = [\boldsymbol{\varphi}_{q+1}^*, \dots, \boldsymbol{\varphi}_{q+m}^*]$, the limit coefficients $\boldsymbol{\alpha}_{(2)}^*(\boldsymbol{\nu}) := \mathbf{U}_{(2)}^{*\top} \mathbf{v}(\boldsymbol{\nu}) \in \mathbb{R}^m$, satisfies*

$$\boldsymbol{\alpha}_{(2)}^*(\boldsymbol{\nu}) = \mathbf{R} \text{ vec}_{\text{sym}} \left(((\mathbf{A}^*)^{-1} \boldsymbol{\alpha}_{(1)}^*(\boldsymbol{\nu})) ((\mathbf{A}^*)^{-1} \boldsymbol{\alpha}_{(1)}^*(\boldsymbol{\nu}))^\top \right) + \mathcal{O}(\|\boldsymbol{\alpha}_{(1)}^*(\boldsymbol{\nu})\|^3), \quad (38)$$

where $\boldsymbol{\alpha}_{(1)}^*(\boldsymbol{\nu})$ is defined in (25), \mathbf{A}^* is defined in (28) and $\mathbf{R} \in \mathbb{R}^{m \times m}$ is defined by,

$$\forall (j, \ell) \in \mathcal{I}, k = 1, \dots, m, \quad \mathbf{R}_{k,(j,\ell)} = \frac{1}{2} (2 - \delta_{j\ell}) \langle \boldsymbol{\varphi}_{q+k}^*, (\mathbf{I} - \Pi_0) \partial_{\nu_j} \partial_{\nu_\ell} U(\mathbf{0}) \rangle.$$

Proof. Projecting the Taylor expansion

$$\mathbf{v}(\boldsymbol{\nu}) = \mathbf{J}_U(\mathbf{0})\boldsymbol{\nu} + \frac{1}{2} D^2 U(\mathbf{0})[\boldsymbol{\nu}, \boldsymbol{\nu}] + \mathcal{O}(\|\boldsymbol{\nu}\|^3) \quad (39)$$

onto $\mathbf{U}_{(1)}^*$ yields $\boldsymbol{\alpha}_{(1)}^*(\boldsymbol{\nu}) = \mathbf{A}^* \boldsymbol{\nu} + \mathcal{O}(\|\boldsymbol{\nu}\|^2)$, hence, following the same lines as in Proposition 2, we deduce $\boldsymbol{\nu} = (\mathbf{A}^*)^{-1} \boldsymbol{\alpha}_{(1)}^*(\boldsymbol{\nu}) + \mathcal{O}(\|\boldsymbol{\alpha}_{(1)}^*(\boldsymbol{\nu})\|^2)$.

Let us now combine the definition $\boldsymbol{\alpha}_{(2)}^*(\boldsymbol{\nu}) := \mathbf{U}_{(2)}^{*\top} \mathbf{v}(\boldsymbol{\nu})$ with (39), and remark that $\mathbf{U}_{(2)}^* \perp \text{Range}(\mathbf{J}_U(\mathbf{0}))$, it follows that the linear term vanishes and

$$\boldsymbol{\alpha}_{(2)}^*(\boldsymbol{\nu}) = \frac{1}{2} \mathbf{U}_{(2)}^{*\top} (\mathbf{I} - \Pi_0) D^2 U(\mathbf{0})[\boldsymbol{\nu}, \boldsymbol{\nu}] + \mathcal{O}(\|\boldsymbol{\nu}\|^3) = \mathbf{R} \text{ vec}_{\text{sym}}(\boldsymbol{\nu} \boldsymbol{\nu}^\top) + \mathcal{O}(\|\boldsymbol{\nu}\|^3).$$

Substituting $\boldsymbol{\nu} = (\mathbf{A}^*)^{-1} \boldsymbol{\alpha}_{(1)}^*(\boldsymbol{\nu}) + \mathcal{O}(\|\boldsymbol{\alpha}_{(1)}^*(\boldsymbol{\nu})\|^2)$ yields the claim. \square

4.3.3 Quadratic law for the *filtered* curvature coefficients

Let $\widehat{\mathbf{U}}_{(2)}^r$ be defined in (34), and \mathcal{C} be defined in (35), from Theorem 9, $\widehat{\mathcal{U}}_{1:m}^{r(2)} = \text{Range}(\widehat{\mathbf{U}}_{(2)}^r)$ converges to \mathcal{C} at rate $\mathcal{O}(r)$. By the discussion in Appendix B (Procrustes alignment), we deduce from (36) that there exists $\mathbf{O}_{(2)}^r \in O(m)$ such that

$$\widehat{\mathbf{U}}_{(2)}^r = \mathbf{U}_{(2)}^* \mathbf{O}_{(2)}^r + \mathbf{E}_2^r, \quad \|\mathbf{E}_2^r\| = \mathcal{O}(r). \quad (40)$$

Moreover, because $\widehat{\mathbf{U}}_{(2)}^r$ is a left singular block of $\widehat{\mathbf{S}}^r = (\mathbf{I} - \Pi_0)\mathbf{S}^r$, we have $\Pi_0 \widehat{\mathbf{U}}_{(2)}^r = 0$. Since also $\Pi_0 \mathbf{U}_{(2)}^* = 0$, it follows that $\Pi_0 \mathbf{E}_2^r = 0$, i.e. $\mathbf{E}_2^r = (\mathbf{I} - \Pi_0)\mathbf{E}_2^r$.

Theorem 11 (Filtered curvature coefficients are homogeneous quadratic in the first-order ones). *The coefficients $\widehat{\alpha}_{(2)}^r(\boldsymbol{\nu}) := \widehat{\mathbf{U}}_{(2)}^{r\top} \mathbf{v}(\boldsymbol{\nu}) \in \mathbb{R}^m$, satisfies uniformly for $\boldsymbol{\nu} \in \mathcal{B}(\mathbf{0}, r)$,*

$$\widehat{\alpha}_{(2)}^r(\boldsymbol{\nu}) = \mathbf{R}^r \text{vec}_{\text{sym}}\left((\mathbf{B}^r \boldsymbol{\alpha}_{(1)}^r(\boldsymbol{\nu}))(\mathbf{B}^r \boldsymbol{\alpha}_{(1)}^r(\boldsymbol{\nu}))^\top\right) + \mathcal{O}\left(r \|\boldsymbol{\alpha}_{(1)}^r(\boldsymbol{\nu})\|^2 + \|\boldsymbol{\alpha}_{(1)}^r(\boldsymbol{\nu})\|^3\right). \quad (41)$$

where $\boldsymbol{\alpha}_{(1)}^r(\boldsymbol{\nu})$ is defined in (24), $\mathbf{R}^r := (\mathbf{O}_{(2)}^r)^\top \mathbf{R} \in \mathbb{R}^{m \times m}$ with the matrix \mathbf{B}^r (resp. \mathbf{R}) in $\mathbb{R}^{m \times m}$ defined in Proposition 2 (resp. in Theorem 10). In particular, the leading term is homogeneous quadratic in $\boldsymbol{\alpha}_{(1)}^r(\boldsymbol{\nu})$, and the remainder is $\mathcal{O}(r^3)$ when $\|\boldsymbol{\nu}\| \leq r$.

Proof. Let us reduce the coefficient to the normal component of $\mathbf{v}(\boldsymbol{\nu})$. Using (40),

$$\begin{aligned} \widehat{\alpha}_{(2)}^r(\boldsymbol{\nu}) &= \widehat{\mathbf{U}}_{(2)}^{r\top} \mathbf{v}(\boldsymbol{\nu}) = (\mathbf{O}_{(2)}^r)^\top \underbrace{\mathbf{U}_{(2)}^{r\top} \mathbf{v}(\boldsymbol{\nu})}_{= \widehat{\alpha}_{(2)}^r(\boldsymbol{\nu})} + \mathbf{E}_2^{r\top} \mathbf{v}(\boldsymbol{\nu}) = (\mathbf{O}_{(2)}^r)^\top \boldsymbol{\alpha}_{(2)}^*(\boldsymbol{\nu}) + \mathbf{E}_2^{r\top} (\mathbf{I} - \Pi_0) \mathbf{v}(\boldsymbol{\nu}). \end{aligned}$$

From the Taylor expansion of \mathbf{v} and $(\mathbf{I} - \Pi_0)\mathbf{J}_U(0) = 0$,

$$(\mathbf{I} - \Pi_0)\mathbf{v}(\boldsymbol{\nu}) = \frac{1}{2} (\mathbf{I} - \Pi_0) D^2 U(0)[\boldsymbol{\nu}, \boldsymbol{\nu}] + \mathcal{O}(\|\boldsymbol{\nu}\|^3) = \mathcal{O}(\|\boldsymbol{\nu}\|^2).$$

Therefore, from (40)

$$\widehat{\alpha}_{(2)}^r(\boldsymbol{\nu}) = (\mathbf{O}_{(2)}^r)^\top \boldsymbol{\alpha}_{(2)}^*(\boldsymbol{\nu}) + \mathcal{O}(\|\boldsymbol{\nu}\|^2). \quad (42)$$

Now we use the limit quadratic law of Theorem 10 :

$$\boldsymbol{\alpha}_{(2)}^*(\boldsymbol{\nu}) = \mathbf{R} \text{vec}_{\text{sym}}(\boldsymbol{\nu} \boldsymbol{\nu}^\top) + \mathcal{O}(\|\boldsymbol{\nu}\|^3),$$

hence (42) gives

$$\widehat{\alpha}_{(2)}^r(\boldsymbol{\nu}) = \mathbf{R}^r \text{vec}_{\text{sym}}(\boldsymbol{\nu} \boldsymbol{\nu}^\top) + \mathcal{O}(r \|\boldsymbol{\nu}\|^2 + \|\boldsymbol{\nu}\|^3), \quad \mathbf{R}^r := (\mathbf{O}_{(2)}^r)^\top \mathbf{R}. \quad (43)$$

Next, we use the expression of $\boldsymbol{\nu}$ in terms of the empirical first-order coefficients (31) and substitute it in the quadratic form $\text{vec}_{\text{sym}}(\boldsymbol{\nu} \boldsymbol{\nu}^\top)$. Since $\text{vec}_{\text{sym}}(\cdot)$ is linear and $\boldsymbol{\nu} \mapsto \boldsymbol{\nu} \boldsymbol{\nu}^\top$ is an square matrix of size m with homogeneous quadratic polynomial entries in $\boldsymbol{\nu}$, we deduce

$$\text{vec}_{\text{sym}}(\boldsymbol{\nu} \boldsymbol{\nu}^\top) = \text{vec}_{\text{sym}}\left((\mathbf{B}^r \boldsymbol{\alpha})(\mathbf{B}^r \boldsymbol{\alpha})^\top\right) + \mathcal{O}(r \|\boldsymbol{\alpha}\|^2 + \|\boldsymbol{\alpha}\|^3),$$

with $\boldsymbol{\alpha} = \boldsymbol{\alpha}_{(1)}^r(\boldsymbol{\nu})$. Combining with (43) and using again $\|\boldsymbol{\nu}\| = \mathcal{O}(\|\boldsymbol{\alpha}\|)$ yields (41). \square

Remark 5 (Unfiltered curvature coefficients). Remark 4 concerns the convergence of the unfiltered curvature modes $\mathbf{U}_{(2)}^r$. Once such convergence holds, an analogous statement can be made at the level of the associated reduced coefficients $\boldsymbol{\alpha}_{(2)}^r(\boldsymbol{\nu})$. Indeed, the asymptotic quadratic dependence established for the *filtered* curvature coefficients in Theorem 11 relies primarily on the convergence of the corresponding singular vectors and on local smoothness arguments. Therefore, if $\mathbf{U}_{(2)}^r$ converges with the same $\mathcal{O}(r)$ rate, the associated coefficients admit an asymptotic expansion of quadratic type with respect to the first block of coefficients $\boldsymbol{\alpha}_{(1)}^r(\boldsymbol{\nu})$ as well.

However, in contrast to the filtered setting, this quadratic dependence is not necessarily *homogeneous*. The absence of tangent-space filtering allows linear terms to persist in the expansion. As a result, the unfiltered curvature coefficients may exhibit a *full quadratic structure*. This observation further motivates, in Section 5, the use of augmented full quadratic models that do not enforce homogeneity a priori.

5 Discussion on quadratic approximation

In Section 4.3, we have shown that, in an SVD-based representation, the second block of coefficients is asymptotically (for small variations of the parameter) quadratic in the first block. This observation provides a theoretical justification for the quadratic ansatz that is used in, e.g., [10, 62, 37], to represent the expressions of the coefficients of the high modes as a function of the coefficients of the low modes. If indeed this is natural in the *Taylor* regime, this has clearly limitations as

- this expansion is valid locally for the variation of the parameter close to a reference value,
- this quadratic expansion calls for a higher-order polynomial ansatz,
- the number of low and high modes is not clear.

In what follows, we recall the basis of these approaches and discuss the points above.

5.1 Description of the quadratic approximation

In this section, we work in $X = \mathbb{R}^{\mathcal{N}}$, using the notation of Section 2, where \mathcal{N} denotes the high-fidelity dimension. We recall that the linear approximation $\tilde{\mathbf{u}}$ of an element $\mathbf{u} \in X$ is given by

$$\tilde{\mathbf{u}} = \mathbf{V}\mathbf{q} \in \mathbb{R}^{\mathcal{N}}, \quad (44)$$

where $\mathbf{V} \in \mathbb{R}^{\mathcal{N} \times n}$ is the reduced basis matrix, $n \ll \mathcal{N}$, and $\mathbf{q} \in \mathbb{R}^n$ is the vector of reduced (generalized) coordinates.

The idea of nonlinear model order reduction methods relies on the notion of sensing number $s_n(\mathcal{S})$ and adds a nonlinear correction term based on a feature map $\Psi : \mathbb{R}^n \rightarrow \mathbb{R}^m$, resulting in an improved approximation (see (16))

$$\tilde{\mathbf{u}} = \mathbf{V}\mathbf{q} + \mathbf{W}\Psi(\mathbf{q}) \in \mathbb{R}^{\mathcal{N}}, \quad (45)$$

with $\mathbf{W} \in \mathbb{R}^{\mathcal{N} \times m}$, where m is the dimension of the nonlinear correction term.

Several nonlinear model reduction methods rely on a homogeneous quadratic feature map given by:

$$\Psi_{\text{hom}} : \mathbb{R}^n \rightarrow \mathbb{R}^m, \quad \mathbf{q} \mapsto \text{vec}_{\text{sym}}(\mathbf{q}\mathbf{q}^\top), \quad m = \frac{n(n+1)}{2}.$$

Two main approaches in the literature employ this map differently. The first, introduced in [10], uses the first n left singular vectors of a snapshot matrix $\mathbf{S} \in \mathbb{R}^{\mathcal{N} \times M}$ as the linear basis \mathbf{V} , and determines the quadratic correction matrix \mathbf{W} by solving the least-squares problem

$$\mathbf{W} = \arg \min_{\mathbf{W}' \in \mathbb{R}^{\mathcal{N} \times m}} \|\mathbf{V}\mathbf{V}^\top \mathbf{S} + \mathbf{W}'\Psi_{\text{hom}}(\mathbf{V}^\top \mathbf{S}) - \mathbf{S}\|_F^2. \quad (46)$$

where $\Psi_{\text{hom}}(\mathbf{V}^\top \mathbf{S}) \in \mathbb{R}^{m \times M}$ denotes the column-wise evaluation of the quadratic feature map applied to the reduced coordinates. We refer to this method as the Quadratic SVD-based Method (QSVD).

A second line of work [62] observes that the SVD/POD basis is not necessarily optimal for a given feature map. The nonlinear decoder Ψ_{hom} operates on the projected data $\mathbf{V}^\top \mathbf{S}$, so if \mathbf{V} is chosen independently of Ψ_{hom} , relevant information may be lost. To address this, the authors propose building \mathbf{V} specifically for the quadratic decoding task through a greedy selection of n vectors from the first $r \gg n$ singular modes. We refer to this approach as the *Quadratic Greedy-based Method* (QGM).

Recalling our Theorem 10 leads to identifying the generalized coordinates with the tangent coefficients $\mathbf{q} \equiv \alpha_1^*(\nu) \in \mathbb{R}^q$ (so that $m = q(q+1)/2$). Indeed, Theorem 10 states

$$\alpha_2^*(\nu) = \mathbf{R} \text{vec}_{\text{sym}}\left((\mathbf{A}^{*-1}\mathbf{q})(\mathbf{A}^{*-1}\mathbf{q})^\top\right) + \mathcal{O}(\|\mathbf{q}\|^3) = \mathbf{R} \text{vec}_{\text{sym}}\left(\mathbf{A}^{*-1}(\mathbf{q}\mathbf{q}^\top)\mathbf{A}^{*-1}\right) + \mathcal{O}(\|\mathbf{q}\|^3).$$

This leads us to introduce the (unique) matrix $\mathbf{T}_{A^*} \in \mathbb{R}^{m \times m}$ such that

$$\text{vec}_{\text{sym}}\left(\mathbf{A}^{*-1}\mathbf{X}\mathbf{A}^{*-1}\right) = \mathbf{T}_{A^*} \text{vec}_{\text{sym}}(\mathbf{X}), \quad \forall \mathbf{X} \in \mathbb{S}^q.$$

where \mathbb{S}^q is the space of real symmetric $q \times q$ matrices. Then

$$\alpha_2^*(\nu) = (\mathbf{R} \mathbf{T}_{A^*}) \operatorname{vec}_{\text{sym}}(\mathbf{q} \mathbf{q}^\top) + \mathcal{O}(\|\mathbf{q}\|^3),$$

and the quadratic-manifold correction matrix in the above ansatz (45) can be identified locally as

$$\mathbf{W} := \mathbf{U}_{(2)}^* \mathbf{R} \mathbf{T}_{A^*}.$$

5.2 Problem formulation

Both approaches employ the quadratic feature map Ψ_{hom} and neglect any affine correction term. However, even asymptotically, as shown in Section 4.3, the affine component in the correction may be non-negligible, and over a wide parameter domain its influence can persist. We illustrate this limitation on a simple 2D toy example, whose columns of the snapshot matrix \mathbf{S} are given by

$$\mathbf{s}_i = \begin{bmatrix} c_1 \alpha \mu^i \\ c_2 (\beta + \gamma(\mu^i)^2) \end{bmatrix}, \quad i = 1, \dots, M, \quad (47)$$

where $\{\mu^i\}_{i=1}^M$ is a symmetric sampling of a centred parametric interval $[-\mu_{\max}, \mu_{\max}]$ (i.e., $\mu^i = -\mu^{M+1-i}$), and the weights satisfy $c_1 > c_2 > 0$. We recall that in both quadratic approaches, an SVD is first performed. It is clear that two modes are needed to capture the solutions in (47). However, nothing guarantees that these modes will be $e_1 = (1, 0)^\top$ and $e_2 = (0, 1)^\top$, nor that the quadratic dependence in the second coordinate will be preserved after the SVD.

To enforce this behavior, we impose the following discrete orthonormality constraints:

$$\frac{1}{M} \sum_{i=1}^M (\alpha \mu^i)^2 = 1, \quad \frac{1}{M} \sum_{i=1}^M (\beta + \gamma(\mu^i)^2)^2 = 1, \quad \frac{1}{M} \sum_{i=1}^M \mu^i (\beta + \gamma(\mu^i)^2) = 0. \quad (48)$$

Because the sampling is symmetric and the interval is centred, the last condition is automatically satisfied provided that $\beta + \gamma(\mu^i)^2$ is an even function of μ^i . In particular, choosing

$$\gamma = -\frac{\beta}{\frac{1}{M} \sum_{i=1}^M (\mu^i)^2} \quad (49)$$

ensures that the second coordinate has zero mean and thus the snapshot matrix \mathbf{S} is centered, i.e.,

$$\bar{\mathbf{s}} = \frac{1}{M} \sum_{i=1}^M \mathbf{s}_i = \mathbf{0}. \quad (50)$$

The remaining parameters α and β are then fixed by the normalization conditions in (48).

Under these assumptions, and thanks to the ordering condition $c_1 > c_2 > 0$, the first two left singular vectors of \mathbf{S} are precisely e_1 and e_2 (see Remark 1). In this setting, we have $n = 1$, $m = 1$, and $N = 2$.

While the linear approximation using N modes and the NCRBA with a quadratic regression model can both recover the full nonlinear behavior, the quadratic methods based solely on the homogeneous map Ψ_{hom} cannot reproduce the constant term $c_2 \beta$ in the second coefficient. This limitation is illustrated in Figure 1.

5.3 Need for full quadratic ansatz

To address the limitation identified in the previous subsection—namely, that the homogeneous quadratic feature map Ψ_{hom} cannot capture affine behaviour—we simply replace it with a full quadratic feature map that includes constant and linear terms. Given $\mathbf{q} \in \mathbb{R}^n$, we define

$$\Psi_{\text{full}}(\mathbf{q}) = \begin{bmatrix} 1 \\ \mathbf{q} \\ \operatorname{vec}_{\text{sym}}(\mathbf{q} \mathbf{q}^\top) \end{bmatrix} \in \mathbb{R}^m, \quad m = 1 + n + \frac{n(n+1)}{2}.$$

This modification integrates directly into both quadratic methods introduced earlier:

- **QSVDM:** the least-squares formulation in (46) remains the same, and one simply replaces Ψ_{hom} by Ψ_{full} .
- **QGM:** the greedy selection procedure and the final step of constructing \mathbf{W} remain identical, except that all evaluations of the decoder use Ψ_{full} instead of Ψ_{hom} .

With this, the approximation (45) takes the form

$$\tilde{\mathbf{u}} = \mathbf{V}\mathbf{q} + \mathbf{C} + \mathbf{L}\mathbf{q} + \mathbf{H} \text{vec}_{\text{sym}}(\mathbf{q}\mathbf{q}^T) \in \mathbb{R}^N, \quad (51)$$

where

$$\mathbf{W} = [\mathbf{C}, \mathbf{L}, \mathbf{H}] \in \mathbb{R}^{N \times m}.$$

We emphasize that, here as well as in the original QSVDM and QGM formulations, nothing guarantees that the columns of \mathbf{W} are linearly independent.

In Figure 1, we illustrate on the toy example (47) that the full quadratic feature map allows both QSVDM and QGM to recover the affine component of the correction, which cannot be captured by the homogeneous quadratic map. This observation is validated again on a more rigorous test case in Section 6.5.

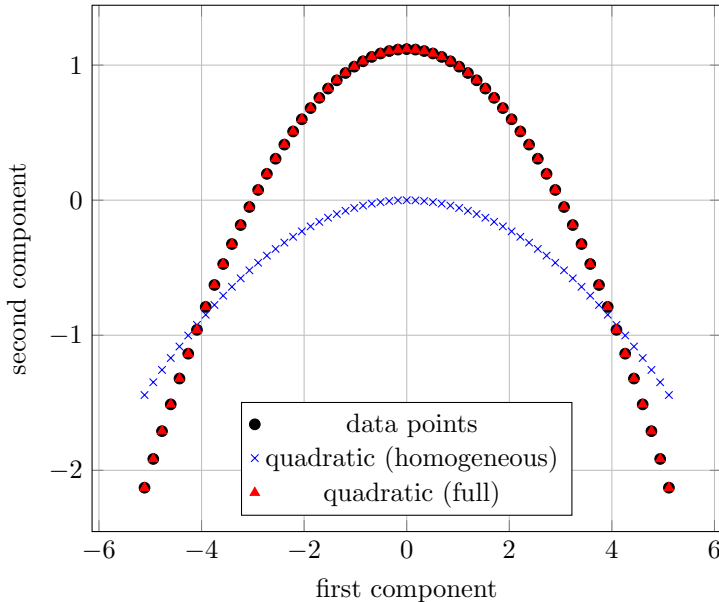


Figure 1: Comparison of quadratic approximation using homogeneous (in blue marks) and full quadratic (in red marks) feature maps on the toy example of section 5.2. The QSVDM and QGM methods are equivalent for this example.

6 Numerical illustrations

This section presents numerical results that illustrate the properties and concepts developed in this work. The experiments are conducted on a representative test case: a parametrized elliptic PDE.

6.1 Test case: A multiparameter problem

We consider the problem of designing a thermal fin to remove heat from a surface effectively, see *e.g.* [57]. The two-dimensional fin, shown in Figure 2, consists of a vertical central **post** and say N_f horizontal **subfins**; the fin conducts heat from a prescribed uniform flux source at the root, Γ_{root} , through the subfins to surrounding flowing air.

The thermal conductivity k_i , for $i = 1, \dots, N_f$ of the i -th subfin (normalized with respect to the post conductivity $k_0 = 1$) may depend on a parameter, *e.g.* $k_i = \mu_i \in [0.1, 10]$, for $i = 1, \dots, p-1$, while $k_i = 1$ for $i = p, \dots, N_f$. The Biot number, which quantifies convective heat transfer to ambient air, is denoted as Bi (larger Bi implies better convection) and may also vary $\text{Bi} = \mu_p \in [0.01, 1]$. The parameter $\boldsymbol{\mu} = (\mu_1, \dots, \mu_p)$ may take values in the compact parameter domain $\mathcal{P} = ([0.1, 10]^{p-1} \times [0.01, 1]) \subset \mathbb{R}^p$.

The full PDE (strong) formulation and boundary conditions are given in [9]. The natural functional space is here $X = H^1(\Omega)$, and we recall here only the corresponding variational formulation: for a given $\boldsymbol{\mu} \in \mathcal{P}$, find $u(\boldsymbol{\mu}) \in X$ such that:

$$a(u(\boldsymbol{\mu}), v; \boldsymbol{\mu}) = f(v), \quad \forall v \in X, \quad (52)$$

where the bilinear and linear forms are given by:

$$a(u, v; \boldsymbol{\mu}) = \sum_{i=0}^{N_f} k_i \int_{\Omega_i} \nabla u \cdot \nabla v \, d\mathbf{x} + \text{Bi} \int_{\Gamma_{\text{ext}}} u v \, d\mathbf{x}, \quad f(v) = \int_{\Gamma_{\text{root}}} v \, d\mathbf{x}.$$

The domains Ω_i and boundaries Γ_{root} and Γ_{ext} are shown in Figure 2, which illustrates the geometry and labeling used in this setup.

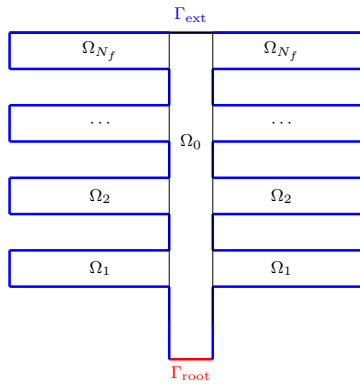


Figure 2: Schematic of thermal fin geometry with labeled subdomains Ω_i and boundaries Γ_{root} , Γ_{ext} .

A finite element (FE) approximation is then applied as a high-fidelity method, where the solution $u(\boldsymbol{\mu}) \in X$ is approximated by $u_{\mathcal{N}}(\boldsymbol{\mu}) \in X_{\mathcal{N}} \subset X$. The solution manifold contained in X (which is not directly computable) is represented by an approximation $\mathcal{S} = \{u_{\mathcal{N}}(\boldsymbol{\mu}), \boldsymbol{\mu} \in \mathcal{P}\} \subset X_{\mathcal{N}}$. To be consistent with Sections 2 and 4, $u_{\mathcal{N}}(\boldsymbol{\mu})$ is represented by its coordinate (degrees of freedom) vector $\mathbf{u}_{\mathcal{N}}(\boldsymbol{\mu})$, allowing \mathcal{S} to be interpreted as a manifold in $X = \mathbb{R}^{\mathcal{N}}$.

6.2 GSS

Here, we perform a comparison between multiple basis construction methods, namely POD, Greedy, and GSS, presented in Section 2. We aim to illustrate the advantages of GSS on the test case described in Section 6.1. For each reduced basis dimension $N \in \{1, \dots, N_{\text{max}} = 56\}$, we compute the projection errors

$$\|\mathbf{u}_{\mathcal{N}}(\boldsymbol{\mu}) - P_{\mathcal{V}_N}(\mathbf{u}_{\mathcal{N}}(\boldsymbol{\mu}))\|_X,$$

for all $\boldsymbol{\mu} \in \mathcal{P}_{\text{test}} \subset \mathcal{P} \subset \mathbb{R}^6$, with $|\mathcal{P}_{\text{test}}| = 1000$. Here, $\mathbf{M} = (a(\zeta_i, \zeta_j; \bar{\boldsymbol{\mu}}))_{i,j=1}^{\mathcal{N}}$ is the mass matrix used to define the X -norm, with $\{\zeta_i\}_{i=1}^{\mathcal{N}}$ denoting the finite element basis functions and $\bar{\boldsymbol{\mu}} = (1, 1, 1, 1, 1, 0.1) \in \mathbb{R}^6$ a fixed reference parameter. Then, in Figure 3, we present the mean and maximum errors over $\mathcal{P}_{\text{test}}$ for each value of N .

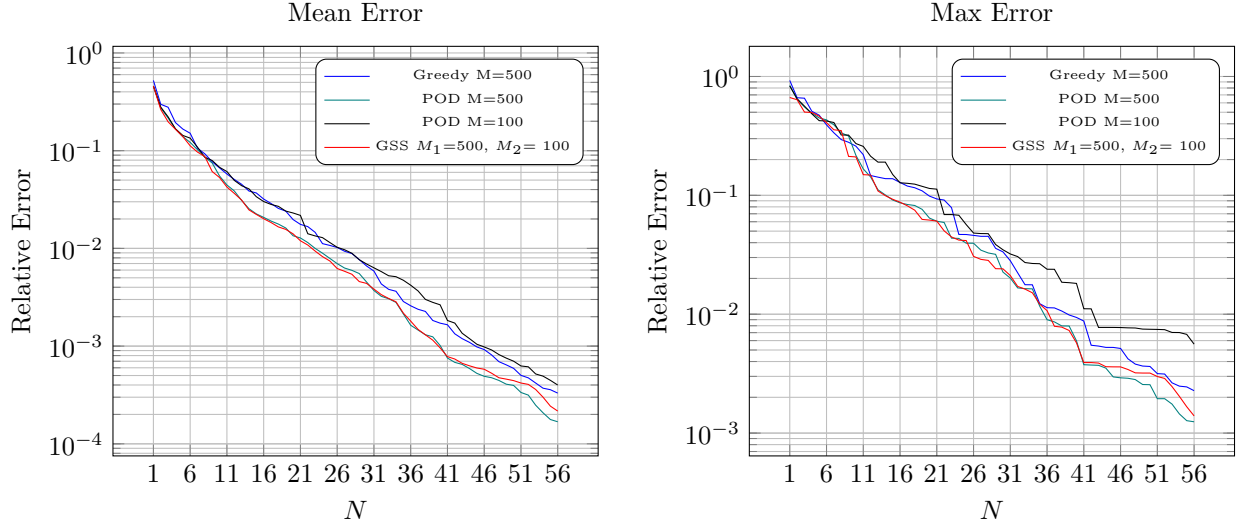


Figure 3: Comparison of mean and max relative errors for different basis construction algorithms.

In this test case, all sampling procedures are performed using a uniform random distribution to construct the training sets for both the Greedy and POD methods.

The improvement of GSS over standard Greedy is visible in both the mean and maximum errors. For instance, to reach a mean error of 10^{-3} , GSS achieves a reduction of approximately 5 basis functions compared to the standard Greedy method. This improvement is attributed to the post-processing SVD/POD compression step.

GSS is also compared with POD using $M = 100$ and $M = 500$ training samples. Since POD requires solving M high-fidelity problems, a fair comparison with GSS using $M_2 = 100$ is against POD with $M = 100$. In this case, GSS exhibits a significant improvement—reducing the mean error by up to 7 modes and the maximum error by up to 15 modes for certain precision levels. This demonstrates that the greedy sampling strategy leads to a more relevant selection of parameters than the uniform sampling used here.

POD with $M = 500$ is included for reference only; it shows that to achieve performance comparable to GSS, one needs $M \gg M_2$, leading to a significantly more expensive procedure.

6.3 Convergence towards the Taylor expansion

Below, we validate numerically the theory developed in Section 4 on the test case 6.1. In particular, we illustrate the convergence results equation (22) and equation (30), as well as the local bijectivity property stated in Theorem 5.

6.3.1 Differentiation with respect to the parameter

To compute the Taylor approximation of a solution near a given parameter, or to represent the tangent plane at a given point, it is essential to differentiate the solution map $u : \boldsymbol{\mu} = (\mu_1, \dots, \mu_p) \mapsto u(\boldsymbol{\mu})$. The differentiability of u follows from the differentiability of the bilinear form $a(\cdot, \cdot; \boldsymbol{\mu})$ with respect to μ_i , $i = 1, \dots, p$ (see [58, 41, 50] Sect. 5.3 for the proof). If we express the bilinear form $a(\cdot, \cdot; \boldsymbol{\mu})$ in (52), in an affine decomposition form:

$$a(u, v; \boldsymbol{\mu}) = \sum_{q=1}^Q \theta_q(\boldsymbol{\mu}) a_q(u, v), \quad (53)$$

then, by differentiating (52), the partial derivative $\frac{\partial u}{\partial \mu_i}(\mu)$ satisfies the following variational problem (since $a(\cdot, \cdot; \boldsymbol{\mu})$ is bilinear and f is independent of $\boldsymbol{\mu}$):

$$a\left(\frac{\partial u}{\partial \mu_i}(\boldsymbol{\mu}), v; \boldsymbol{\mu}\right) = - \sum_{q=1}^Q \frac{\partial \theta_q}{\partial \mu_i}(\boldsymbol{\mu}) a_q(u(\boldsymbol{\mu}), v), \quad \forall v \in X. \quad (54)$$

For higher-order derivatives, one must differentiate the variational problem recursively to obtain a new variational problem for each derivative. Similarly to what was done for the variational problem (52), a FE approximation of the derivatives in X_N can be obtained using a Galerkin approach.

6.3.2 Convergence of the SVD modes

In 4.2, we showed that the first p SVD modes $\mathbf{U}_{(1)}^r$ of the centered snapshot matrix \mathbf{S}^r converge, up to an orthogonal transformation, as $r \rightarrow 0$, to the SVD modes $\mathbf{U}_{(1)}^*$ of the matrix $\mathbf{J}_U(\mathbf{0}) \cdot \mathbf{P}$, which span the tangent space T_0^* . This convergence, stated in equation (22) and illustrated in Figure 4, is linear in r , *i.e.*, $\mathcal{O}(r)$. We note that when $r^2 \leq \epsilon$, rounding errors are expected to dominate the total error, where ϵ is approximately 10^{-16} in double precision. Additionally, for certain specific samplings, the convergence rate can improve. For instance, for $p = 1$, if $\sum_{i=1}^M (\mu^i)^3 = 0$, the convergence is $\mathcal{O}(r^2)$, whereas in general, it remains $\mathcal{O}(r)$ as mentioned before.

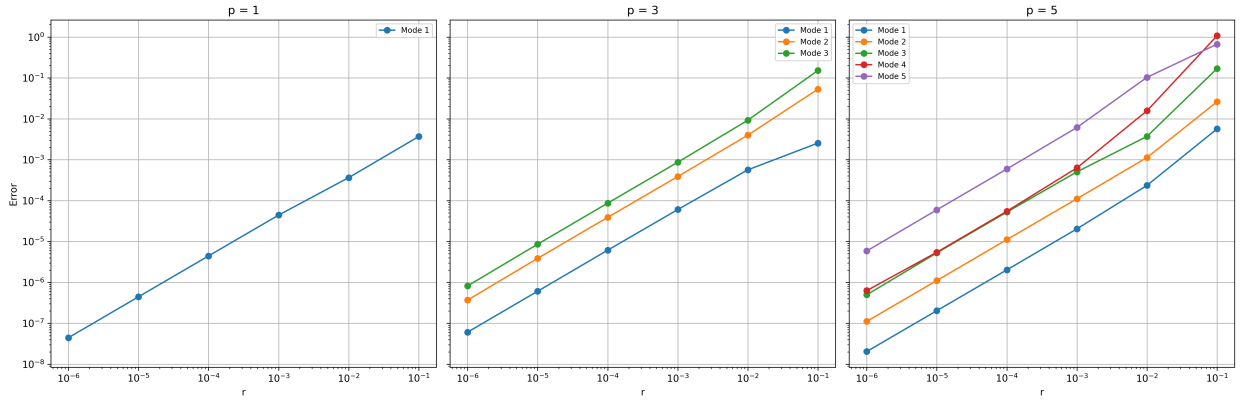


Figure 4: Convergence of the first p SVD modes of \mathbf{S}^r for dimension $p \in \{1, 3, 5\}$.

Similarly, in Figures 5 and 6, we illustrate the numerical convergence of the second block of $m = \frac{p(p+1)}{2}$ left singular vectors of the snapshot matrix \mathbf{S}^r toward the curvature modes discussed in Section 4.3.

In the filtered case, where the projection $(\mathbf{I} - \Pi_0)$ removes the tangent contribution, the first m singular vectors $\widehat{\mathbf{U}}_{(2)}^r$ of the projected matrix $\widehat{\mathbf{S}}^r$ converge to the modes $\mathbf{U}_{(2)}^*$ that span the curvature subspace \mathcal{C} at the expected linear rate $\mathcal{O}(r)$.

In the non-filtered case, we observe a similar convergence behavior for the second block of modes $\mathbf{U}_{(2)}^r$ of \mathbf{S}^r , even though a rigorous proof is not yet established.

Furthermore, we note that for $r^4 \leq \epsilon$, roundoff errors are expected to influence the numerical results, limiting the observed convergence rate.

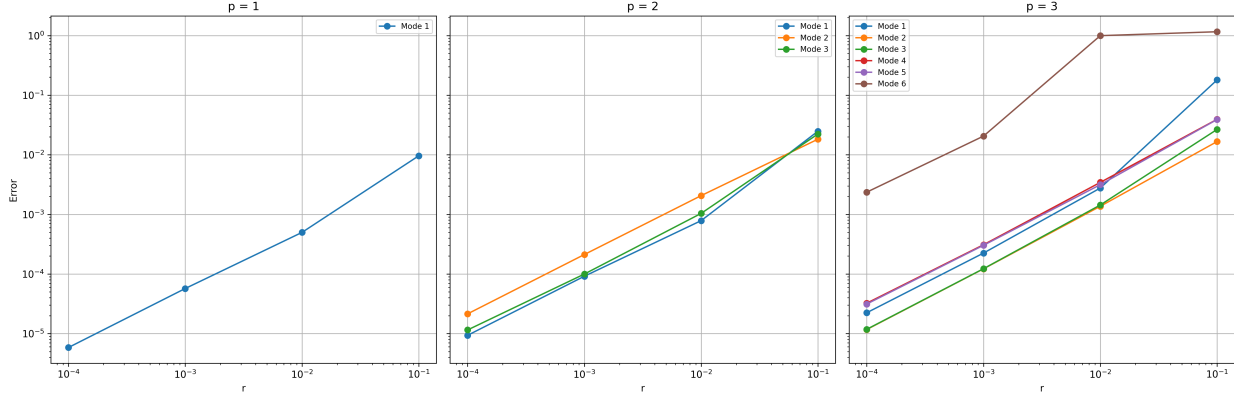


Figure 5: Convergence of the first m SVD modes of $\widehat{\mathbf{S}}^r = (\mathbf{I} - \Pi_0)\mathbf{S}^r$ for dimension $p \in \{1, 2, 3\}$.

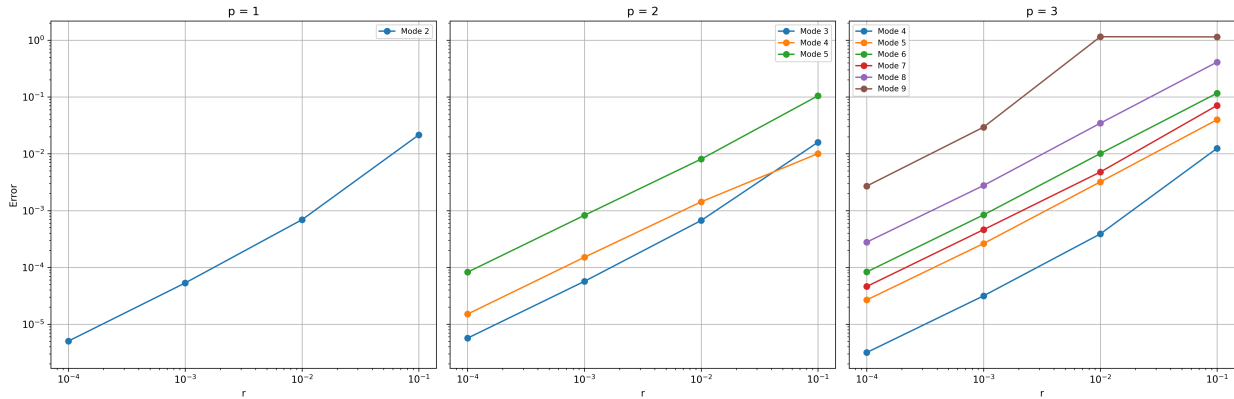


Figure 6: Convergence of the second block of SVD modes of \mathbf{S}^r for dimension $p \in \{1, 2, 3\}$.

6.4 Recovering the high RB modes from the low ones

In the following numerical experiments, the Biot number varies in the interval $[0.01, 1]$ and the thermal conductivities k_i in $[0.1, 10]$ for $i = 1, \dots, 5$. For the case $p = 1$, we vary only the Biot number while keeping the thermal conductivities fixed. For $p > 1$, we vary the conductivities k_i for $i = 1, \dots, p - 1$, in addition to the Biot number.

Thanks to the bijection established (locally) in Section 4.2.3, the parameter μ and therefore the higher coefficients $\{\alpha_k(\mu)\}_{k=n+1}^N$ can be inferred directly from the first n coefficients. Accordingly, for $k = n + 1, \dots, N$, the following relation holds:

$$\alpha_k(\mu) = \psi^k(\alpha_1(\mu), \dots, \alpha_n(\mu)),$$

where each ψ^k denotes a nonlinear function.

In Sections 4.2 and 6.3.2, we showed that one can locally choose $n = p$ when working with a centered manifold $\mathcal{S} - u^*$. However, in the global formulation — *i.e.*, when approximating \mathcal{S} directly — one may need to choose $n = p + 1$ even in a local neighborhood, *i.e.*, in a small parametric domain \mathcal{P} . In the following numerical experiments, we adopt the latter non-centered approach.

Another fundamental step is the approximation of the functions ψ^k , which constitutes a regression task. The goal is to learn a nonlinear map $\psi : \mathbb{R}^n \rightarrow \mathbb{R}^{N-n}$ such that:

$$\widehat{\psi}(\alpha_1, \dots, \alpha_n) \approx (\alpha_{n+1}, \dots, \alpha_N) = (\psi^{n+1}(\alpha_1, \dots, \alpha_n), \dots, \psi^N(\alpha_1, \dots, \alpha_n)) \quad (55)$$

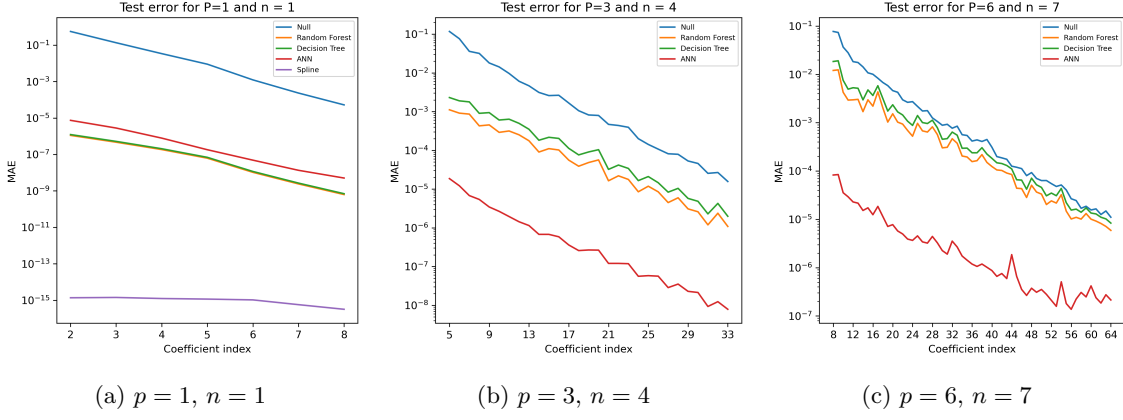


Figure 7: Mean absolute error on a test set for different ML models and $p \in \{1, 3, 6\}$. Each panel shows the comparison of various regression models (decision trees, random forests, splines, polynomial regression, and neural networks) for different parameter dimensions.

For this task, we tested several classical machine learning models, namely decision trees, random forests, splines, polynomial regression, and neural networks. These models are trained offline on a dataset of size 9×10^5 . Importantly, this dataset is generated using the classical RBM and is independent of the high-fidelity dimension \mathcal{N} . In figure 7, for the univariate case ($p = 1, n = 1$, panel 7a), spline regression achieves the best accuracy, although other models also reach a mean relative error around 10^{-5} . In the multivariate setting ($p > 1$, panels 7b and 7c), where learning models based on splines perform poorly (due to the curse of dimensionality), neural networks outperform the other models and exhibit greater robustness to increasing dimensionality. Two main considerations guide the choice of the regression model. The first is accuracy, as the total error is primarily driven by the regression error. The second is the inference cost, which matters in the online phase. For this latter aspect, decision trees or parallelized random forests are favorable options, as their inference complexity depends mainly on the depth of the trees.

6.5 Enhanced approximation with full quadratic ansatz

In this section, we apply the quadratic approximation methods introduced in Section 5.1, as well as the augmented full quadratic feature map proposed in Section 5.3, to the test case described in Section 6.1. As is suggested in [62], the snapshot matrix is first centered by subtracting its empirical mean, and the reduction is performed on this mean-free data.

The goal is not to assess or promote the efficiency of the quadratic manifold approximations, but rather to demonstrate that, whenever such methods are employed, there is no reason to discard the affine terms in the reduced coefficients. This is clearly illustrated in Figure 8: using the augmented feature map improves the reconstruction, yielding up to one order of accuracy compared to the purely homogeneous quadratic map. The magnitude of this gain naturally depends on the problem, but the example shows that constant and linear contributions in the correction cannot, in general, be ignored.

Note that, for some applications, the centering preprocessing step can be crucial for the performance of quadratic approximation methods. This is notably the case for the advecting wave test case considered in [62], where the preprocessing centering step is explicitly performed and documented (in the given implementation) as having a strong impact on the performance of QGM. While homogeneous quadratic feature maps fail to compensate for non-centered data, the augmented full quadratic feature map naturally accounts for such affine effects.

It is also worth noting that, unlike the NCRBA, whose effective reduced dimension satisfies $n \approx n_s$, quadratic approximation methods require $n \gg n_s$ to perform adequately over wide parameter ranges. Consequently, they are not expected to be competitive in such regimes. For an extensive comparison between these methods, we refer to [8].

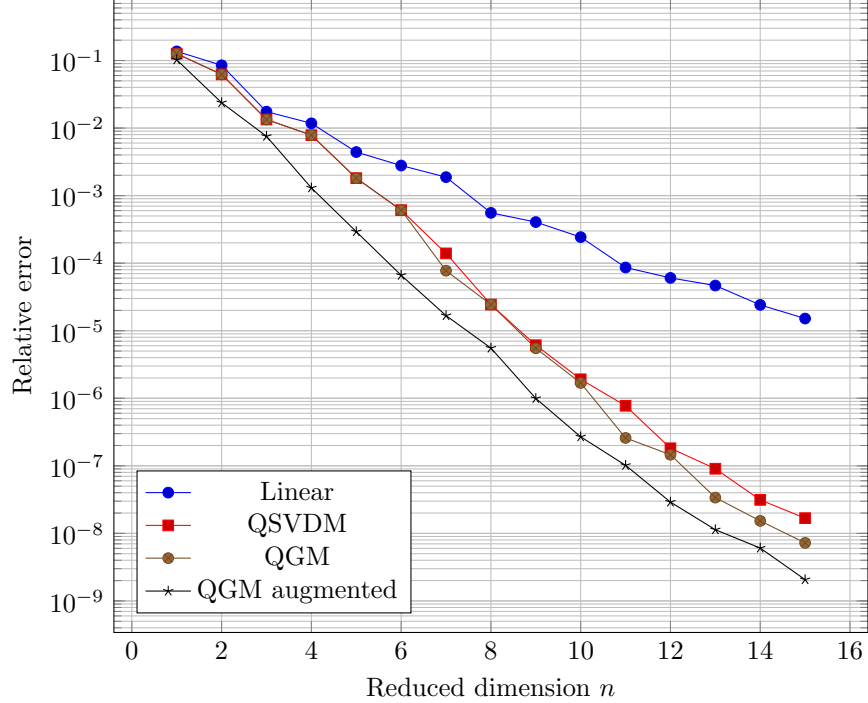


Figure 8: Relative approximation errors of the linear approximation and the different quadratic variants as the reduced dimension n increases. The parametric dependence involves two parameters, $\text{Bi} \in [0.01, 1]$ and $k_1 \in [0.1, 10]$.

7 Conclusion

This paper contributes to the development of nonlinear reduced-basis approximation methods. More specifically, we focus on techniques that, in the spirit of the Gelfand widths framework, rely on approximations expressed as a truncated expansion with N terms that has been named the Nonlinear Compressive Reduced Basis Approximation.

In this representation, the first n terms correspond to genuine unknowns—i.e., degrees of freedom (dof) of the discrete problem to be solved—while the remaining $\bar{n} = N - n$ terms are expressed explicitly in terms of the first n dof.

We first prove that, if the underlying problem depends on p parameters, locally the choice $n = p$ is the right one when a centered expansion is chosen (see subsection 2.1). By continuity, this shows that it is sufficient to choose $n \geq p$, with n of the order of p , in order to characterize the approximation properly. The total number of terms N , and hence \bar{n} , is then selected solely to ensure the desired approximation accuracy, which is itself related to the Kolmogorov linear dimension. Note that this result is associated with the inverse problem: is it possible to retrieve μ from the knowledge of the RB coefficients $\alpha_{i,\mu}$, $i = 1, \dots, n$, see (16) ?

Since the construction of the (linear) reduced basis is a problem in its own right—traditionally addressed either through a singular value decomposition (SVD) approach or through greedy algorithms—we propose, in subsection 6.2, as a side result, a hybrid strategy that combines the advantages of both methods to further improve the quality of the reduced basis.

The second major contribution of this article is to explain why expressing the high modes as quadratic functions of the low modes arises naturally, but this quadratic relationship is only valid locally. Consequently, to achieve accurate approximations over a wide range of parameter variations, it is necessary to consider more complex representations. These may be provided, for instance, by statistical learning (AI-based) approaches or by more sophisticated functional expressions, such as those proposed in [13].

Finally, the theory developed in this work delineates what can be achieved at a purely theoretical level, namely the selection of n as a function of p to solve the above inverse problem, together with explicit

expressions of the coefficients indexed from $n + 1$ to N as a function of the first n ones. In practice, however, for a prescribed target accuracy $\varepsilon > 0$, the approximation error must be interpreted as the combination of two distinct contributions :

- The first contribution is associated with the truncation level N of the linear expansion used to represent the approximation, whether in an SVD basis or in a more suitable reduced basis.
- The second contribution arises from the approximation error incurred when expressing the high-mode coefficients as functions of the n low-mode coefficients.

When this latter dependence is obtained via a learning-based procedure whose accuracy depends on the size of the available dataset, the resulting error is inherently relative. Consequently, for a fixed dataset, the absolute error on the reconstructed coefficients improves as the magnitude of these coefficients decreases. This practical constraint naturally leads to selecting values of n that may exceed the theoretical limit—of order p —suggested by the analysis presented in this paper.

Therefore, practical considerations, and in particular the use of a posteriori error estimators, must be regarded as a necessary complement to the theoretical framework developed here. The systematic incorporation of such tools lies beyond the scope of the present work and is the subject of ongoing investigations.

A Different notions of principal angles and the connection with Davis–Kahan $\sin \Theta$ Theorem

Principal Angles (Canonical Angles) between Subspaces. Let \mathcal{U} and \mathcal{V} be two subspaces of \mathbb{R}^n with $\dim(\mathcal{U}) = \dim(\mathcal{V}) = p$. The *principal angles* (also called *canonical angles*) $\theta_1, \theta_2, \dots, \theta_p \in [0, \pi/2]$ between \mathcal{U} and \mathcal{V} are defined via the singular value decomposition (SVD). Let $\mathbf{Q}_{\mathcal{U}} \in \mathbb{R}^{n \times p}$ and $\mathbf{Q}_{\mathcal{V}} \in \mathbb{R}^{n \times p}$ be matrices whose columns form orthonormal bases of \mathcal{U} and \mathcal{V} , respectively. Consider the $p \times p$ matrix $\mathbf{Q}_{\mathcal{U}}^T \mathbf{Q}_{\mathcal{V}}$. Its singular values, $\sigma_1, \sigma_2, \dots, \sigma_p$, (in nonincreasing order $\sigma_1 \geq \sigma_2 \geq \dots \geq \sigma_p \geq 0$) are the cosines of the principal angles. In particular, we define

$$\cos \theta_i = \sigma_i(\mathbf{Q}_{\mathcal{U}}^T \mathbf{Q}_{\mathcal{V}}) \quad (i = 1, \dots, p),$$

so that $0 \leq \theta_1 \leq \theta_2 \leq \dots \leq \theta_p \leq \frac{\pi}{2}$. It is often convenient to collect these angles into a diagonal matrix

$$\Theta(\mathcal{U}, \mathcal{V}) = \text{diag}(\theta_1, \dots, \theta_p),$$

together with the associated matrices

$$\sin \Theta(\mathcal{U}, \mathcal{V}) = \text{diag}(\sin \theta_1, \dots, \sin \theta_p), \quad \cos \Theta(\mathcal{U}, \mathcal{V}) = \text{diag}(\cos \theta_1, \dots, \cos \theta_p).$$

This matrix notation is the one commonly used in perturbation theory.

Geometrical interpretation. Geometrically, θ_1 is the smallest angle between any unit vector in \mathcal{U} and any unit vector in \mathcal{V} , θ_2 is the next smallest after "removing" the directions that achieved θ_1 (more precisely by working in the intersections of \mathcal{U} and \mathcal{V} with the orthogonal complement of these directions), and so on, up to θ_p which is the largest angle. Equivalently, one can characterize θ_1 variationally as

$$\cos \theta_1 = \max_{\mathbf{u} \in \mathcal{U}, \mathbf{v} \in \mathcal{V}} \frac{\mathbf{u}^T \mathbf{v}}{\|\mathbf{u}\| \|\mathbf{v}\|}$$

and θ_1 is attained by some unit vectors $\mathbf{u}_1 \in \mathcal{U}$, $\mathbf{v}_1 \in \mathcal{V}$ (called the *first principal vectors*). Then recursively for $i = 2, \dots, p$,

$$\cos \theta_i = \max_{\substack{\mathbf{u} \in \mathcal{U}, \mathbf{v} \in \mathcal{V}, \\ \mathbf{u} \perp \mathbf{u}_1, \dots, \mathbf{u}_{i-1} \\ \mathbf{v} \perp \mathbf{v}_1, \dots, \mathbf{v}_{i-1}}} \frac{\mathbf{u}^T \mathbf{v}}{\|\mathbf{u}\| \|\mathbf{v}\|}$$

with corresponding principal vectors $\mathbf{u}_i, \mathbf{v}_i$ in the subspaces orthogonal to the previous ones. In particular, θ_p (the largest principal angle) corresponds to the least aligned directions between \mathcal{U} and \mathcal{V} .

If \mathcal{U} and \mathcal{V} share a nonzero intersection, then $\theta_1 = 0$; at the other extreme, if \mathcal{U} is orthogonal to \mathcal{V} (every $\mathbf{u} \in \mathcal{U}$ is orthogonal to every $\mathbf{v} \in \mathcal{V}$), then $\theta_p = \frac{\pi}{2}$ (and $\cos \theta_p = 0$). More generally, principal angles characterize the relative orientation of \mathcal{U} and \mathcal{V} in \mathbb{R}^n in an invariant way (independent of the particular bases chosen for \mathcal{U} and \mathcal{V}). They also coincide with the concept of canonical correlations in statistics (the cosines $\cos \theta_i = \sigma_i$ are the *canonical correlation* coefficients between the subspaces spanned by $\mathbf{Q}_{\mathcal{U}}$ and $\mathbf{Q}_{\mathcal{V}}$).

It is interesting to note that the optimality conditions associated with the above max-problem lead to the following orthogonality conditions :

$$\forall i, j, \quad i, j = 1, \dots, p \quad \mathbf{u}_i^T \mathbf{u}_j = \delta_{i,j}, \quad \mathbf{u}_i^T \mathbf{v}_j = \delta_{i,j} \cos \theta_i$$

From the above orthogonality conditions, a direct characterization of the maximum angle can be stated :

$$\cos \theta_p = \min_{\substack{\mathbf{u} \in \mathcal{U}, \mathbf{v} \in \mathcal{V} \\ \|\mathbf{u}\| = \|\mathbf{v}\| = 1}} \max_{\substack{\mathbf{w} \in \mathcal{U} \cap \mathbf{u}^\perp, \mathbf{z} \in \mathcal{V} \cap \mathbf{v}^\perp \\ \mathbf{w} \neq 0, \mathbf{z} \neq 0}} \frac{|(\mathbf{u} + \mathbf{w})^T (\mathbf{v} + \mathbf{z})|}{\|\mathbf{u} + \mathbf{w}\| \|\mathbf{v} + \mathbf{z}\|},$$

that allows to define θ_p without involving the previous angles.

Remark (Matrices or sets of vectors). The above definition applies equally to the column spaces (ranges) of two matrices, or to two sets of vectors, since these span subspaces. In practice, given two matrices \mathbf{A} and \mathbf{B} with column-space $\mathcal{U} = \text{Range}(\mathbf{A})$ and $\mathcal{V} = \text{Range}(\mathbf{B})$, one often computes an orthonormal basis for each (for example via QR factorization) and then obtains the principal angles between \mathcal{U} and \mathcal{V} via the SVD of $\mathbf{Q}_{\mathcal{U}}^T \mathbf{Q}_{\mathcal{V}}$. The same procedure works for two arbitrary finite sets of vectors spanning \mathcal{U} and \mathcal{V} . Thus, we will speak of principal angles between subspaces, or between matrices \mathbf{A} and \mathbf{B} , or between sets of vectors, interchangeably – the notion depends only on the two subspaces in question.

Extreme Angles and Distance Between Subspaces. The smallest principal angle θ_1 indicates the closest alignment between \mathcal{U} and \mathcal{V} , whereas the largest principal angle θ_p indicates the worst-case misalignment. A useful quantitative measure of distance between subspaces is given by the largest principal angle. Indeed, $\sin \theta_p$ can be interpreted as the operator norm distance between the two subspaces on the Grassmann manifold. To make this precise, let $\mathbf{P}_{\mathcal{U}}$ and $\mathbf{P}_{\mathcal{V}}$ denote the orthogonal projection matrices onto \mathcal{U} and \mathcal{V} , respectively. It can be shown that

$$\sin \theta_p = \|(\mathbf{I} - \mathbf{P}_{\mathcal{U}})\mathbf{P}_{\mathcal{V}}\|_2 = \|(\mathbf{I} - \mathbf{P}_{\mathcal{V}})\mathbf{P}_{\mathcal{U}}\|_2.$$

In other words, $\sin \theta_p$ equals the operator norm of the difference between the two projection operators $\mathbf{P}_{\mathcal{U}}$ and $\mathbf{P}_{\mathcal{V}}$ (this difference $\mathbf{P}_{\mathcal{U}} - \mathbf{P}_{\mathcal{V}}$ has the same singular values as $(\mathbf{I} - \mathbf{P}_{\mathcal{U}})\mathbf{P}_{\mathcal{V}}$). To see the intuition behind this fact, observe that for any unit vector $\mathbf{v} \in \mathcal{V}$, the quantity $\|\mathbf{v} - \mathbf{P}_{\mathcal{U}}\mathbf{v}\| = \|(\mathbf{I} - \mathbf{P}_{\mathcal{U}})\mathbf{v}\|$ is the distance from \mathbf{v} to the subspace \mathcal{U} . The maximum of this distance (over all $\mathbf{v} \in \mathcal{V}$ with $\|\mathbf{v}\| = 1$) is achieved when \mathbf{v} is the principal vector corresponding to θ_p . For that vector, $\mathbf{v} - \mathbf{P}_{\mathcal{U}}\mathbf{v}$ is a unit vector orthogonal to \mathcal{U} , meaning \mathbf{v} is as “far” from \mathcal{U} as possible. Thus

$$\max_{\mathbf{v} \in \mathcal{V}, \|\mathbf{v}\| = 1} \|\mathbf{v} - \mathbf{P}_{\mathcal{U}}\mathbf{v}\| = \sin \theta_p.$$

By symmetry, the same holds with \mathcal{U} and \mathcal{V} swapped. This quantity $\sin \theta_p$ is sometimes called the gap between subspaces \mathcal{U} and \mathcal{V} . It provides a natural measure of distance on the Grassmannian (the space of all p -dimensional subspaces of \mathbb{R}^n). For example, $\sin \theta_p = 0$ if and only if $\mathcal{U} = \mathcal{V}$, and $\sin \theta_p = 1$ if and only if \mathcal{U} is orthogonal to \mathcal{V} .

Davis–Kahan $\sin \Theta$ Theorem (Eigenvector Perturbation). Principal angles play a key role in perturbation bounds for invariant subspaces. A cornerstone result is the Davis–Kahan $\sin \Theta$ theorem, which gives an upper bound on the largest principal angle between two eigenspaces in terms of the perturbation norm. In one convenient form, it can be stated as follows. Let \mathbf{A} be a real symmetric matrix and $\tilde{\mathbf{A}} = \mathbf{A} + \mathbf{E}$ be a perturbed version (with \mathbf{E} symmetric as well). Suppose \mathcal{U} is an invariant subspace of \mathbf{A} spanned by p eigenvectors of \mathbf{A} (say, associated with eigenvalues $\lambda_1, \dots, \lambda_p$), and let $\tilde{\mathcal{U}}$ be the p -dimensional invariant subspace of $\tilde{\mathbf{A}}$ spanned by the corresponding p eigenvectors of $\tilde{\mathbf{A}}$ (with eigenvalues denoted $\tilde{\lambda}_1, \dots, \tilde{\lambda}_p$). The Davis–Kahan theorem asserts that if the perturbed eigenvalues remain separated from the chosen eigenvalue cluster of \mathbf{A} by a positive gap, namely

$$\delta = \min \left\{ |\lambda_i - \tilde{\lambda}_j| : 1 \leq i \leq p, \quad p+1 \leq j \leq n \right\} > 0,$$

then the subspace $\tilde{\mathcal{U}}$ (the perturbed eigenspace) stays close to \mathcal{U} ; more quantitatively, the largest principal angle θ_p between \mathcal{U} and $\tilde{\mathcal{U}}$ is bounded by

$$\|\sin \Theta(\mathcal{U}, \tilde{\mathcal{U}})\|_2 = \sin \theta_p(\mathcal{U}, \tilde{\mathcal{U}}) \leq \frac{\|\mathbf{E}\|_2}{\delta}.$$

In the above, $\|\cdot\|_2$ denotes the operator norm (spectral norm), and the same results hold for the Frobenius norm

$$\|\sin \Theta(\mathcal{U}, \tilde{\mathcal{U}})\|_F \leq \frac{\|\mathbf{E}\|_F}{\delta}.$$

A useful practical variant replaces the two-sided gap δ by an easily computable one-sided gap involving only the eigenvalues of \mathbf{A} . Let $\delta^* = \min\{|\lambda_i - \lambda_j| : 1 \leq i \leq p, p+1 \leq j \leq n\}$ denote the separation between the selected eigenvalue cluster of \mathbf{A} and the remainder of its spectrum. When the perturbation is sufficiently small so that $\|\mathbf{E}\|_2 < \delta^*$, one obtains the following bound

$$\|\sin \Theta(\mathcal{U}, \tilde{\mathcal{U}})\|_F \leq \frac{2\|\mathbf{E}\|_F}{\delta^*}.$$

This classical result is often referred to as the $\sin \Theta$ theorem of Davis and Kahan (1970) [25]. It provides a concise and powerful way to bound the perturbation of an invariant subspace in terms of the perturbation of the matrix. We emphasize that the $\sin \Theta$ theorem applies specifically to symmetric (Hermitian) matrices; analogous bounds for non-symmetric or rectangular matrices involve singular vectors and utilize extensions due, e.g., to Wedin (1972), but those are beyond our present scope. (Here we restrict to the real, symmetric case as it suffices for our purposes).

B SVD modes convergence

In this appendix, we discuss the convergence behavior of the left singular vectors (SVD modes) of a perturbed matrix $\mathbf{A}^r \in \mathbb{R}^{n \times m}$ converging to a fixed matrix $\mathbf{A} \in \mathbb{R}^{n \times m}$ as $r \rightarrow 0$ with $\|\mathbf{A}^r - \mathbf{A}\| = \mathcal{O}(r)$. We assume that $\text{rank}(\mathbf{A}) = p$.

B.1 Problem statement

Let the singular value decompositions be given by

$$\mathbf{A}^r = \mathbf{U}^r \boldsymbol{\Sigma}^r (\mathbf{Z}^r)^\top, \quad \mathbf{A} = \mathbf{U} \boldsymbol{\Sigma} \mathbf{Z}^\top,$$

with

$$\boldsymbol{\Sigma}^r = \text{diag}(\sigma_1^r, \dots, \sigma_p^r, \dots), \quad \boldsymbol{\Sigma} = \text{diag}(\sigma_1, \dots, \sigma_p, 0, \dots),$$

where $\sigma_1 \geq \dots \geq \sigma_p > 0$, and $\sigma_p^r > 0$ for all sufficiently small r (Weyl's theorem). We are particularly interested in the first p left singular vectors

$$\mathbf{U}_{(1)}^r := \mathbf{U}_{(:,1:p)}^r = [\boldsymbol{\varphi}_1^r, \dots, \boldsymbol{\varphi}_p^r], \quad \mathbf{U}_{(1)} := \mathbf{U}_{(:,1:p)} = [\boldsymbol{\varphi}_1, \dots, \boldsymbol{\varphi}_p],$$

and we ask whether

$$\|\mathbf{U}_{(1)}^r - \mathbf{U}_{(1)}\| \rightarrow 0,$$

as $r \rightarrow 0$.

B.2 Non-uniqueness of SVD modes

The above question is subtle because the singular vectors are not uniquely defined. Two cases are of interest:

1. **Simple singular value:** If σ_j is simple, then the corresponding singular vector is unique only up to a sign flip. That is, both $\boldsymbol{\varphi}_j$ and $-\boldsymbol{\varphi}_j$ are valid singular vectors.

2. **Multiple singular values:** If $\sigma_j = \dots = \sigma_{j+k-1}$ is repeated, then the associated singular vectors span a subspace of dimension k . Any orthonormal basis of this subspace is valid, so the singular vectors are determined only up to a $k \times k$ orthogonal transformation.

Thus, the matrix of singular vectors is only defined up to multiplication by an orthogonal transformation. Concretely, if $\mathbf{U}'_{(1)} \in \mathbb{R}^{n \times p}$ is another valid choice of left singular vectors associated with the same singular values, then there exists an orthogonal matrix $\mathbf{O} \in \mathbb{R}^{p \times p}$ such that

$$\mathbf{U}'_{(1)} = \mathbf{U}_{(1)} \mathbf{O}.$$

B.3 Convergence up to orthogonal transformation

For any two choices of SVD bases $\mathbf{U}'_{(1)}, \mathbf{U}_{(1)} \in \mathbb{R}^{n \times p}$, Davis–Kahan $\sin \Theta$ theorem ensures that the subspaces spanned by $\mathbf{U}'_{(1)}$ and $\mathbf{U}_{(1)}$ converge:

$$\|\sin \Theta(\mathbf{U}'_{(1)}, \mathbf{U}_{(1)})\|_F = \mathcal{O}(r).$$

Hence, one can expect that there exists a sequence of orthogonal matrices $\mathbf{O}_{(1)}^r \in O(p)$ such that

$$\|\mathbf{U}'_{(1)} - \mathbf{U}_{(1)} \mathbf{O}_{(1)}^r\|_F = \mathcal{O}(r).$$

One can even go further by explicitly searching for the *best* orthogonal transformation of $\mathbf{U}_{(1)}$ that aligns it as closely as possible with $\mathbf{U}'_{(1)}$. Note that the corresponding transformed basis $\mathbf{U}_{(1)} \mathbf{O}_{(1)}^r$ does not necessarily correspond to an SVD basis, but it provides the optimal alignment in the least-squares sense. This problem is precisely the classical *orthogonal Procrustes problem*:

$$\mathbf{O}_{(1)}^r = \arg \min_{\mathbf{O} \in O(p)} \|\mathbf{U}'_{(1)} - \mathbf{U}_{(1)} \mathbf{O}\|_F^2.$$

The solution is obtained via the SVD of

$$\mathbf{U}_{(1)}^\top \mathbf{U}'_{(1)} = \mathbf{P}^r \mathbf{D}^r (\mathbf{Q}^r)^\top,$$

namely

$$\mathbf{O}_{(1)}^r = \mathbf{P}^r (\mathbf{Q}^r)^\top.$$

With this alignment, one obtains

$$\|\mathbf{U}'_{(1)} - \mathbf{U}_{(1)} \mathbf{O}_{(1)}^r\|_F \leq \sqrt{2} \|\sin \Theta(\mathbf{U}'_{(1)}, \mathbf{U}_{(1)})\|_F = \mathcal{O}(r).$$

Acknowledgments

As part of the “France 2030” initiative, this work has benefited from a national grant managed by the French National Research Agency (Agence Nationale de la Recherche), attributed to the ExaMA project of the NumPEEx PEPR program under reference ANR-22-EXNU-0002, and has also been partially funded by the European Research Council (ERC) under the European Union’s Horizon 2020 research and innovation program (grant No. 810367), project EMC2 (YM).

References

- [1] Eddie Aamari and Clément Levraud. Nonasymptotic rates for manifold, tangent space and curvature estimation. *The Annals of Statistics*, 47(1):177–204, 2019.
- [2] Shady E Ahmed and Omer San. Breaking the kolmogorov barrier in model reduction of fluid flows. *Fluids*, 5(1):26, 2020.
- [3] David Amsallem and Charbel Farhat. An online method for interpolating linear parametric reduced-order models. *SIAM Journal on Scientific Computing*, 33(5):2169–2198, 2011.
- [4] David Amsallem, Matthew J Zahr, and Charbel Farhat. Nonlinear model order reduction based on local reduced-order bases. *International Journal for Numerical Methods in Engineering*, 92(10):891–916, 2012.
- [5] Alberto Badías, David González, Iciar Alfaro, Francisco Chinesta, and Elias Cueto. Local proper generalized decomposition. *International Journal for Numerical Methods in Engineering*, 112(12):1715–1732, 2017.
- [6] Oleg Balabanov, Matthias Beaupère, Laura Grigori, and Victor Lederer. Block subsampled randomized hadamard transform for low-rank approximation on distributed architectures. *arXiv preprint arXiv:2210.11295*, 2022.
- [7] Oleg Balabanov and Anthony Nouy. Randomized linear algebra for model reduction. part i: Galerkin methods and error estimation. *Advances in Computational Mathematics*, 45(5):2969–3019, 2019.
- [8] Hassan Ballout, Yvon Maday, and Christophe Prud’Homme. Combined galerkin and regression based algorithm for parameter dependant pde’s. *Hal preprint hal-05143191*, 2025.
- [9] Hassan Ballout, Yvon Maday, and Christophe Prud’homme. Nonlinear compressive reduced basis approximation for multi-parameter elliptic problem. In *Multiscale, Nonlinear and Adaptive Approximation II*, pages 55–73. Springer, 2024.
- [10] Joshua Barnett and Charbel Farhat. Quadratic approximation manifold for mitigating the Kolmogorov barrier in nonlinear projection-based model order reduction. *Journal of Computational Physics*, 464:111348, 2022.
- [11] Joshua Barnett, Charbel Farhat, and Yvon Maday. Neural-network-augmented projection-based model order reduction for mitigating the Kolmogorov barrier to reducibility. *Journal of Computational Physics*, 492:112420, 2023.
- [12] Peter Benner, Serkan Gugercin, and Karen Willcox. A survey of projection-based model reduction methods for parametric dynamical systems. *SIAM review*, 57(4):483–531, 2015.
- [13] Antoine Bensalah, Anthony Nouy, and Joel Soffo. Nonlinear manifold approximation using compositional polynomial networks. *arXiv preprint arXiv:2502.05088*, 2025.
- [14] Florian Bernard, Angelo Iollo, and Sébastien Riffaud. Reduced-order model for the bgk equation based on pod and optimal transport. *Journal of Computational Physics*, 373:545–570, 2018.
- [15] Marie Billaud-Friess, Arthur Macherey, Anthony Nouy, and Clémentine Prieur. A probabilistic reduced basis method for parameter-dependent problems. *Advances in Computational Mathematics*, 50(2):19, 2024.
- [16] Peter Binev, Albert Cohen, Wolfgang Dahmen, Ronald DeVore, Guergana Petrova, and Przemyslaw Wojtaszczyk. Convergence rates for greedy algorithms in reduced basis methods. *SIAM journal on mathematical analysis*, 43(3):1457–1472, 2011.
- [17] Jeff Borggaard, Zhu Wang, and Lizette Zietsman. A goal-oriented reduced-order modeling approach for nonlinear systems. *Computers & Mathematics with Applications*, 71(11):2155–2169, 2016.

[18] Tan Bui-Thanh, Karen Willcox, and Omar Ghattas. Model reduction for large-scale systems with high-dimensional parametric input space. *SIAM Journal on Scientific Computing*, 30(6):3270–3288, 2008.

[19] Giuseppe Carere, Maria Strazzullo, Francesco Ballarin, Gianluigi Rozza, and Rob Stevenson. A weighted pod-reduction approach for parametrized pde-constrained optimal control problems with random inputs and applications to environmental sciences. *Computers & Mathematics with Applications*, 102:261–276, 2021.

[20] Kevin Carlberg. Adaptive h-refinement for reduced-order models. *International Journal for Numerical Methods in Engineering*, 102(5):1192–1210, 2015.

[21] Sridhar Chellappa, Lihong Feng, and Peter Benner. A training set subsampling strategy for the reduced basis method. *Journal of Scientific Computing*, 89(3):63, 2021.

[22] Albert Cohen, Wolfgang Dahmen, Ronald DeVore, and James Nichols. Reduced basis greedy selection using random training sets. *ESAIM: Mathematical Modelling and Numerical Analysis*, 54(5):1509–1524, 2020.

[23] Albert Cohen and Ronald DeVore. Kolmogorov widths under holomorphic mappings. *IMA Journal of Numerical Analysis*, 36(1):1–12, 2016.

[24] Albert Cohen, Charbel Farhat, Yvon Maday, and Agustin Somacal. Nonlinear compressive reduced basis approximation for pdes. *Comptes Rendus. Mécanique*, 351(S1):357–374, 2023.

[25] Chandler Davis and W. M. Kahan. The rotation of eigenvectors by a perturbation. iii. *SIAM Journal on Numerical Analysis*, 7(1):1–46, 1970.

[26] S Ares de Parga, Radek Tezaur, Carlos G Hernández, and Charbel Farhat. Nonlinear projection-based model order reduction with machine learning regression for closure error modeling in the latent space. *arXiv preprint arXiv:2507.00634*, 2025.

[27] Ronald DeVore, Guergana Petrova, and Przemyslaw Wojtaszczyk. Greedy algorithms for reduced bases in banach spaces. *Constructive Approximation*, 37(3):455–466, 2013.

[28] Ronald A DeVore. Nonlinear approximation. *Acta Numerica*, 7:51–150, 1998.

[29] Ronald A DeVore, Ralph Howard, and Charles Micchelli. Optimal nonlinear approximation. *Manuscripta Mathematica*, 63:469–478, 1989.

[30] Markus Dihlmann, Martin Drohmann, and Bernard Haasdonk. Model reduction of parametrized evolution problems using the reduced basis method with adaptive time-partitioning. *Proc. of ADMOS*, 2011:64, 2011.

[31] Virginie Ehrlacher, Damiano Lombardi, Olga Mula, and François-Xavier Vialard. Nonlinear model reduction on metric spaces. application to one-dimensional conservative pdes in wasserstein spaces. *ESAIM: Mathematical Modelling and Numerical Analysis*, 54(6):2159–2197, 2020.

[32] Andrea Ferrero, Tommaso Taddei, and Lei Zhang. Registration-based model reduction of parameterized two-dimensional conservation laws. *Journal of Computational Physics*, 457:111068, 2022.

[33] Nicola Franco, Andrea Manzoni, and Paolo Zunino. A deep learning approach to reduced order modelling of parameter dependent partial differential equations. *Mathematics of Computation*, 92(340):483–524, 2023.

[34] Stefania Fresca, Luca Dede', and Andrea Manzoni. A comprehensive deep learning-based approach to reduced order modeling of nonlinear time-dependent parametrized pdes. *Journal of Scientific Computing*, 87(2):61, 2021.

[35] Rudy Geelen, Laura Balzano, Stephen Wright, and Karen Willcox. Learning physics-based reduced-order models from data using nonlinear manifolds. *Chaos: An Interdisciplinary Journal of Nonlinear Science*, 34(3), 2024.

[36] Rudy Geelen and Karen Willcox. Localized non-intrusive reduced-order modelling in the operator inference framework. *Philosophical Transactions of the Royal Society A*, 380(2229):20210206, 2022.

[37] Rudy Geelen, Stephen Wright, and Karen Willcox. Operator inference for non-intrusive model reduction with quadratic manifolds. *Computer Methods in Applied Mechanics and Engineering*, 403:115717, 2023.

[38] Jean-Frédéric Gerbeau and Damiano Lombardi. Approximated lax pairs for the reduced order integration of nonlinear evolution equations. *Journal of Computational Physics*, 265:246–269, 2014.

[39] Anna C Gilbert and Kevin O’Neill. CA-PCA: Manifold dimension estimation, adapted for curvature. *arXiv preprint arXiv:2309.13478*, 2023. Published version in SIAM Journal on Mathematics of Data Science.

[40] Nathan Halko, Per-Gunnar Martinsson, and Joel A Tropp. Finding structure with randomness: Probabilistic algorithms for constructing approximate matrix decompositions. *SIAM review*, 53(2):217–288, 2011.

[41] Jan S Hesthaven, Gianluigi Rozza, Benjamin Stamm, et al. *Certified reduced basis methods for parametrized partial differential equations*, volume 590. Springer, 2016.

[42] Philip Holmes. *Turbulence, coherent structures, dynamical systems and symmetry*. Cambridge university press, 2012.

[43] Angelo Iollo and Damiano Lombardi. Advection modes by optimal mass transfer. *Physical Review E*, 89(2):022923, 2014.

[44] Angelo Iollo and Tommaso Taddei. Point-set registration in bounded domains via the fokker–planck equation. *Comptes Rendus. Mathématique*, 363(G8):809–824, 2025.

[45] Shobhit Jain, Paolo Tiso, Johannes B Rutzmoser, and Daniel J Rixen. A quadratic manifold for model order reduction of nonlinear structural dynamics. *Computers & Structures*, 188:80–94, 2017.

[46] Boris Kramer, Benjamin Peherstorfer, and Karen E. Willcox. Learning nonlinear reduced models from data with operator inference. *Annual Review of Fluid Mechanics*, 56(1):521–548, 2024.

[47] Pierre Ladevèze. On reduced models in nonlinear solid mechanics. *European Journal of Mechanics-A/Solids*, 60:227–237, 2016.

[48] Kookjin Lee and Kevin T. Carlberg. Model reduction of dynamical systems on nonlinear manifolds using deep convolutional autoencoders. *Journal of Computational Physics*, 404:108973, 2020.

[49] Hannah Lu and Daniel M Tartakovsky. Lagrangian dynamic mode decomposition for construction of reduced-order models of advection-dominated phenomena. *Journal of Computational Physics*, 407:109229, 2020.

[50] Yvon Maday and A Patera. Reduced basis methods. *Model Order Reduction; Benner, P., Grivet-Talocia, S., Quarteroni, A., Rozza, G., Schilders, W., Silveira, L., Eds*, pages 139–179, 2020.

[51] Yvon Maday and Benjamin Stamm. Locally adaptive greedy approximations for anisotropic parameter reduced basis spaces. *SIAM Journal on Scientific Computing*, 35(6):A2417–A2441, 2013.

[52] Rambod Mojgani and Maciej Balajewicz. Lagrangian basis method for dimensionality reduction of convection dominated nonlinear flows. *arXiv preprint arXiv:1701.04343*, 2017.

[53] Mario Ohlberger and Stephan Rave. Nonlinear reduced basis approximation of parameterized evolution equations via the method of freezing. *Comptes Rendus Mathématique*, 351(23-24):901–906, 2013.

- [54] Benjamin Peherstorfer. Model reduction for transport-dominated problems via online adaptive bases and adaptive sampling. *SIAM Journal on Scientific Computing*, 42(5):A2803–A2836, 2020.
- [55] Benjamin Peherstorfer. Breaking the Kolmogorov barrier with nonlinear model reduction. *Notices of the American Mathematical Society*, 69(5):725–733, 2022.
- [56] I. Pesenson. Estimates of Kolmogorov, Gelfand and linear n-widths on compact Riemannian manifolds. *Proceedings of the American Mathematical Society*, 144(7):2985–2998, 2016.
- [57] Christophe Prud'homme, Dimitrios Rovas, Karen Veroy, Luc Machiels, Yvon Maday, Anthony T. Patera, and Gabriel Turinici. Reliable real-time solution of parametrized partial differential equations: Reduced-basis output bound methods. *J. Fluids Eng.*, 124(1):70–80, 2002.
- [58] Alfio Quarteroni, Andrea Manzoni, and Federico Negri. *Reduced basis methods for partial differential equations: An introduction*. 2015.
- [59] Julius Reiss, Philipp Schulze, Jörn Sesterhenn, and Volker Mehrmann. The shifted proper orthogonal decomposition: A mode decomposition for multiple transport phenomena. *SIAM Journal on Scientific Computing*, 40(3):A1322–A1344, 2018.
- [60] Donsub Rim, Benjamin Peherstorfer, and Kyle T Mandli. Manifold approximations via transported subspaces: Model reduction for transport-dominated problems. *SIAM Journal on Scientific Computing*, 45(1):A170–A199, 2023.
- [61] Omer San and Jeff Borggaard. Principal interval decomposition framework for pod reduced-order modeling of convective boussinesq flows. *International Journal for Numerical Methods in Fluids*, 78(1):37–62, 2015.
- [62] Paul Schwerdtner and Benjamin Peherstorfer. Greedy construction of quadratic manifolds for nonlinear dimensionality reduction and nonlinear model reduction, 2024.
- [63] Lawrence Sirovich. Turbulence and the dynamics of coherent structures. i. coherent structures. *Quarterly of applied mathematics*, 45(3):561–571, 1987.
- [64] Tommaso Taddei. A registration method for model order reduction: data compression and geometry reduction. *SIAM Journal on Scientific Computing*, 42(2):A997–A1027, 2020.
- [65] Hemant Tyagi, Elif Vural, and Pascal Frossard. Tangent space estimation for smooth embeddings of riemannian manifolds. *Information and Inference: A Journal of the IMA*, 2(1):69–114, 2013.
- [66] Piermario Vitullo, Alessio Colombo, Nicola Rares Franco, Andrea Manzoni, and Paolo Zunino. Nonlinear model order reduction for problems with microstructure using mesh informed neural networks. *Finite Elements in Analysis and Design*, 229:104068, 2024.